



Nonlinear secondary resonance of FG porous silicon nanobeams under periodic hard excitations based on surface elasticity theory

Banghua Xie¹ · Saeid Sahmani² · Babak Safaei³ · Bin Xu¹

Received: 8 February 2019 / Accepted: 30 December 2019 / Published online: 21 January 2020
© Springer-Verlag London Ltd., part of Springer Nature 2020

Abstract

To impart desirable material properties, functionally graded (FG) porous silicon has been produced in which the porosity changes gradually across the material volume. The prime objective of this work is to predict the influence of the surface free energy on the nonlinear secondary resonance of FG porous silicon nanobeams under external hard excitations. On the basis of the closed-cell Gaussian-random field scheme, the mechanical properties of the FG porous material are achieved corresponding to the uniform and three different FG patterns of porosity dispersion. The Gurtin–Murdoch theory of elasticity is implemented into the classical beam theory to construct a surface elastic beam model. Thereafter, with the aid of the method of multiple time-scales together with the Galerkin technique, the size-dependent nonlinear differential equations of motion are solved corresponding to various immovable boundary conditions and porosity dispersion patterns. The frequency response and amplitude response associated with the both subharmonic and superharmonic hard excitations are obtained including multiple vibration modes and interactions between them. It is found that for the subharmonic excitation, the nanobeam is excited within a specific range of the excitation amplitude, and this range shifts to higher excitation amplitude by incorporating the surface free energy effects. For the superharmonic excitation, by taking surface stress effect into account, the excitation amplitude associated with the peak of the vibration amplitude enhances. Moreover, in the subharmonic case, it is demonstrated that by increasing the porosity coefficient, the value of the excitation frequency at the joint point of the two branches of the frequency-response curve reduces. In the superharmonic case, it is revealed that an increment in the value of porosity coefficient leads to decrease the peak of the oscillation amplitude and the associated excitation frequency.

Keywords Functionally graded materials · Size dependency · Porosity · Nonlinear dynamics · Multiple time-scales method

1 Introduction

As a novel functionally graded (FG) material, FG porous material have acquired a significant attention in recent years due to its improved characteristics such as flexibility of tailoring a desired design and excellent capability for energy dissipation and biomedical applications. Chen et al.

[1] explored the nonlinear free vibrations of sandwich Timoshenko beams with FG porous core with different porosity distributions. Wang and Wu [2] performed a free vibration analysis for FG porous cylindrical shell subjected to various types of immovable boundary conditions. Wu et al. [3] used a computational scheme based on the finite element method to predict the free and forced vibration responses of FG porous beams. Karami et al. [4] investigated the size-dependent guided wave propagation in mounted FG porous nanoplates. Sahmani et al. [5–7] developed a size-dependent beam model for nonlinear mechanical behaviors of FG porous micro/nanobeams reinforced with graphene platelets. Gao et al. [8] presented an analytical solution on the basis of the method of multiple scales for the nonlinear primary resonance of FG porous cylindrical shells. Safaei et al. [9–11] analyzed the

✉ Saeid Sahmani
s.sahmani@ug.edu.ge

¹ School of Civil Engineering & Architecture, Nanchang Institute of Technology, Nanchang 330099, Jiangxi, China

² School of Science and Technology, The University of Georgia, 0171 Tbilisi, Georgia

³ School of Mechanical Engineering, Eastern Mediterranean University, G. Magosa, TRNC Mersin 10, Turkey

thermoelastic response of carbon-nanotube-reinforced sandwich plates. Qin et al. [12, 13] developed a unified solution for traveling wave analysis and vibrations of FG shallow shells under general boundary conditions.

Several unconventional continuum theories of elasticity have been proposed and employed to take different size dependencies into consideration [14–48]. Gurtin and Murdoch [49, 50] developed a theoretical framework based on the continuum mechanics including surface stress effect which has an excellent capability to incorporate the surface stress effect into the mechanical responses of nanostructures. Based on this type of continuum elasticity theory, the surface is simulated as a mathematical layer of zero thickness with different material properties derived from the underlying bulk material. A variety of problems at nanoscale have been analyzed on the basis of Gurtin–Murdoch elasticity theory. Herein, some of the investigations carried out about the effect of surface energy on the mechanical behaviors of nanostructures are cited.

Wang and Feng [51] investigated the free vibration response of microscale beam including surface effects on the basis of Euler–Bernoulli and Timoshenko beam theories, respectively. Lü et al. [52] presented a generalized refined theory incorporating the influence of surface stress for functionally graded films based on Gurtin–Murdoch elasticity theory. Fu et al. [53] studied the influences of surface energy on the free vibration and buckling behavior of nanobeams in both linear and nonlinear regimes using Galerkin technique. Ansari and Sahmani [54, 55] analyzed the surface stress effect on the free vibrations of nanoplates and bending of nanobeams. Gao et al. [56] considered the surface stress effect in the buckling analysis of nanowires on elastomeric substrates. Sahmani et al. [57] studied the free vibration characteristics of postbuckled functionally graded third-order shear deformable nanobeams using surface elasticity theory. Asemi and Farajpour [58] presented a vibration analysis of circular graphene sheets subjected to a thermo-mechanical loading condition based on the surface elasticity theory. Sahmani et al. [59] used Gurtin–Murdoch elasticity theory to develop a non-classical beam model to study the nonlinear forced vibrations of nanobeams including surface effects. Ghorbanpour Arani et al. [60] explored the surface stress effect on vibrations of bioliquid-filled microtubules embedded in cytoplasm. Sahmani et al. [61–63] examined the surface free energy effect on the nonlinear buckling and postbuckling behavior of cylindrical nanoshells under various loading conditions. Lu et al. [64] developed surface elastic Kirchhoff and Mindlin plate models for dynamic response of nanoplates. Sun et al. [65] presented an analytical solution for buckling of piezoelectric cylindrical nanoshells under combination of compressive mechanical loads and external voltages including surface stress effect. Attia and Abel Rahman [31]

investigated the free vibration response of FG viscoelastic nanobeams based on the surface elasticity theory. Sarafraz et al. [66] studied the nonlinear secondary resonance of a silicon nanobeam on the basis of the surface elastic beam model. Dong et al. [67] proposed a refined beam model to describe the buckling characteristics of hollow metal nanowires encapsulating carbon nanotubes. Sahmani et al. [68] predicted the surface stress effect on the nonlinear buckling and postbuckling of cylindrical nanoshells under hydrostatic pressure. Lu et al. [69] introduced a unified size-dependent plate model including surface stress effect for buckling analysis of nanoplates. Yang et al. [70] analyzed a mode-III nanocrack at the interface between two bonded dissimilar under antiplane shear loading. Sahmani et al. [71] developed a surface elastic shell model for the nonlinear primary resonance of FG porous nanoshells including modal interactions.

The objective of the present study is to analyze the nonlinear secondary resonance of FG porous silicon nanobeams under hard excitation in the presence of surface free energy effects. Consequently, the Gurtin–Murdoch theory of elasticity is applied to the classical Euler–Bernoulli beam theory to construct a surface elastic beam model. With the aid of the multiple time scales method together with the Galerkin technique, the size-dependent nonlinear differential equation of motion is solved incorporating multiple vibration modes and interactions between them. The frequency response and amplitude response associated with the both subharmonic and superharmonic excitations are obtained corresponding to various beam thicknesses, boundary conditions, porosity coefficients and porosity dispersion patterns.

2 FG porous beam model based on the surface elasticity

As it is displayed in Fig. 1, four different patterns for porosity dispersion are taken into consideration including the uniform porous material (Pattern A), and three FG porous materials with patterns B, C, and D. As a result, the Young's modulus (E), shear modulus (G), and mass density (ρ) of the porous nanobeams can be extracted for each pattern as below

$$\begin{aligned} E(z) &= \tilde{E}[1 - \Gamma_p s(z)] \\ G(z) &= \frac{E(z)}{(2[1 - \nu(z)])} \\ \rho(z) &= \tilde{\rho}[1 - \Gamma_m s(z),] \end{aligned} \quad (1)$$

where

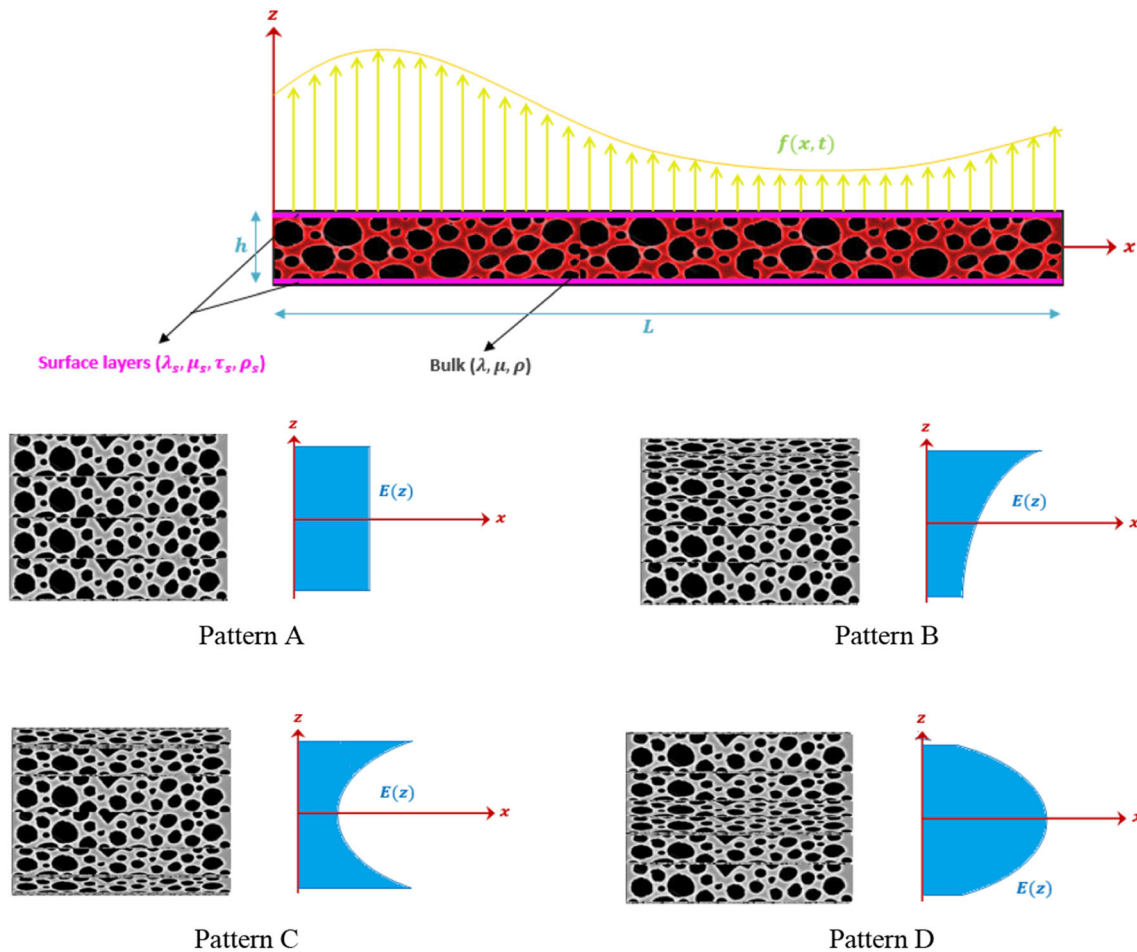


Fig. 1 Schematic representation of FG porous silicon nanobeam with surface layers under hard excitation

$$s(z) = \begin{cases} s_0 & \text{for pattern A} \\ \cos\left(\frac{\pi z}{2h} + \frac{\pi}{4}\right) & \text{for pattern B} \\ \cos\left(\frac{\pi z}{h}\right) & \text{for pattern C} \\ 1 - \cos\left(\frac{\pi z}{h}\right) & \text{for pattern D} \end{cases} \quad (2)$$

where \tilde{E} and $\tilde{\rho}$ represent the maximum Young’s modulus and maximum mass density of the FG porous silicon nanobeam.

On the basis of the Gaussian-random field scheme [72], all finite dimensional distributions are supposed to be multivariate normal distributions for any number of coordinates. Therefore, the mass density coefficient (Γ_m) can be introduced as a function of the porosity coefficient (Γ_p) as below:

$$\Gamma_m = 1.121 \left[1 - (1 - \Gamma_p s(z))^{1/2.3} \right] / s(z). \quad (3)$$

In addition, the Poisson’s ratio of the FG porous silicon can be obtained for each type of porosity dispersion pattern

via the closed-cell Gaussian-random field scheme [58] as follows:

$$v(z) = 0.221 \left(1 - \frac{\rho(z)}{\tilde{\rho}} \right) + \tilde{v} \left[1 + 0.342 \left(1 - \frac{\rho(z)}{\tilde{\rho}} \right)^2 - 1.21 \left(1 - \frac{\rho(z)}{\tilde{\rho}} \right) \right]. \quad (4)$$

The proper value of s_0 should be defined in such a way that the mass density of FG porous silicon becomes equal for all four different porosity dispersion patterns. Therefore, one will have

$$s_0 = \frac{1}{\Gamma_p} \left[1 - \left(\frac{\frac{1}{h} \int_{-\frac{h}{2}}^{\frac{h}{2}} \frac{\rho(z)}{\tilde{\rho}} dz + 0.121}{1.121} \right)^{2.3} \right]. \quad (5)$$

In accordance with Fig. 1, an FG porous silicon nanobeam of length L , width b and thickness h under harmonic excitation is considered. It is assumed that the nanobeam consists of a bulk part and additional thin outer surface

layers. Within the framework of the classical Euler–Bernoulli beam theory, the displacement field including mid-plane stretching effect can be expressed as

$$u_x(x, t) = u(x, t) - z \frac{\partial w(x, t)}{\partial x}, \quad u_z(x, t) = w(x, t), \quad (6)$$

where w denotes the middle surface displacements along z -axis, u represents the mid-plane stretching, and t stands for time.

Following the von Karman kinematics of nonlinearity, the strain–displacement relationship including the mid-plane stretching can be written as

$$\epsilon_{xx} = \frac{\partial u}{\partial x} - z \frac{\partial^2 w}{\partial x^2} + \frac{1}{2} \left(\frac{\partial w}{\partial x} \right)^2. \quad (7)$$

Based upon the elastic constitutive law, the stress component related to the bulk part of the FG porous silicon nanobeam can be given as

$$\sigma_{xx} = [\lambda(z) + 2\mu(z)] \left(\frac{1}{2} \left(\frac{\partial w}{\partial x} \right)^2 + \frac{\partial u}{\partial x} - z \frac{\partial^2 w}{\partial x^2} \right) \quad (8)$$

in which $\lambda(z) = E(z)v(z)/[1 - v^2(z)]$, $\mu(z) = E(z)/[2(1 + v(z))]$ are Lamé’s constants.

About the atomic features of nanostructures, there are always interactions between the elastic surface and bulk material. As a result, in-plane loads in various directions are applied to nanostructures. These in-plane loads on the free surface of a nanobeam make surface stresses. In accordance with Gurtin–Murdoch theory of elasticity, the surface stress components can be introduced in the following form [49, 50]

$$\begin{aligned} \sigma_{ij}^s &= \tau_s \delta_{ij} + (\tau_s + \lambda_s) \epsilon_{kk} \delta_{ij} + 2(\mu_s - \tau_s) \epsilon_{ij} + \tau_s u_{i,j}^s; \quad (i, j = x, y), \\ \sigma_{iz}^s &= \tau_s u_{z,i}^s \end{aligned} \quad (9)$$

where λ_s and μ_s denote the surface Lamé’s constants and τ_s represents the residual surface stress under unstrained conditions. Consequently, the surface stress components for an FG porous silicon nanobeam can be achieved in terms of the displacement components as follows

$$\begin{aligned} \sigma_{xx}^s &= (\lambda_s + 2\mu_s) \left(\frac{1}{2} \left(\frac{\partial w}{\partial x} \right)^2 + \frac{\partial u}{\partial x} - z \frac{\partial^2 w}{\partial x^2} \right) + \tau_s - \frac{\tau_s}{2} \left(\frac{\partial w}{\partial x} \right)^2 \\ \sigma_{xz}^s &= \tau_s \frac{\partial w}{\partial x} \end{aligned} \quad (10)$$

In the classical continuum elasticity, it is assumed that $\sigma_{zz} = 0$, because this component of stress is so small compared to other ones. Nevertheless, this assumption does not satisfy the balance conditions on the free surface layer. To tackle this problem, it is supposed that the stress component σ_{zz} varies linearly through the thickness and

satisfies the equilibrium necessities on the free surface of an FG porous silicon nanobeam. As a result, it yields

$$\begin{aligned} \sigma_{zz} &= \frac{\left(\frac{\partial \sigma_{xz}^{s+}}{\partial x} - \rho_s^+ \frac{\partial^2 w}{\partial t^2} \right) + \left(\frac{\partial \sigma_{xz}^{s-}}{\partial x} - \rho_s^- \frac{\partial^2 w}{\partial t^2} \right)}{2} \\ &\quad + \frac{\left(\frac{\partial \sigma_{xz}^{s+}}{\partial x} - \rho_s^+ \frac{\partial^2 w}{\partial t^2} \right) - \left(\frac{\partial \sigma_{xz}^{s-}}{\partial x} - \rho_s^- \frac{\partial^2 w}{\partial t^2} \right)}{h} z, \end{aligned} \quad (11)$$

where ρ_s is the surface mass density.

By inserting Eq. (10) in Eq. (11), one will have

$$\sigma_{zz} = \frac{2z}{h} \left(\tau_s \frac{\partial^2 w}{\partial x^2} - \rho_s \frac{\partial^2 w}{\partial t^2} \right), \quad (12)$$

Thereafter, substitution σ_{zz} into the constitutive Eq. (8) yields

$$\begin{aligned} \sigma_{xx} &= [\lambda(z) + 2\mu(z)] \left(\frac{1}{2} \left(\frac{\partial w}{\partial x} \right)^2 + \frac{\partial u}{\partial x} - z \frac{\partial^2 w}{\partial x^2} \right) \\ &\quad + \frac{2v(z)z}{(1 - v(z))h} \left(\tau_s \frac{\partial^2 w}{\partial x^2} - \rho_s \frac{\partial^2 w}{\partial t^2} \right) \end{aligned} \quad (13)$$

Based upon the surface continuum theory of elasticity, the total strain energy of an FG porous nanobeam in the present of surface free energy effects can be expressed as

$$\begin{aligned} \Pi_s &= \frac{1}{2} \int_x \int_S \sigma_{ij} \epsilon_{ij} dx dS + \frac{1}{2} \left(\int_{S^+} \sigma_{ij}^s \epsilon_{ij} dS^+ + \int_{S^-} \sigma_{ij}^s \epsilon_{ij} dS^- \right) \\ &= \frac{1}{2} \int_x \left\{ (N_{xx} + \bar{N}_{xx}) \left(\frac{1}{2} \left(\frac{\partial w}{\partial x} \right)^2 + \frac{\partial u}{\partial x} \right) - (M_{xx} + \bar{M}_{xx}) \frac{\partial^2 w}{\partial x^2} \right\} dx, \end{aligned} \quad (14)$$

in which

$$\begin{aligned} N_{xx} &= b \int_{-\frac{h}{2}}^{\frac{h}{2}} \sigma_{xx} dz = A_{11} \left(\frac{1}{2} \left(\frac{\partial w}{\partial x} \right)^2 + \frac{\partial u}{\partial x} \right) - B_{11} \frac{\partial^2 w}{\partial x^2} \\ \bar{N}_{xx} &= \bar{A}_{11} \left(\frac{1}{2} \left(\frac{\partial w}{\partial x} \right)^2 + \frac{\partial u}{\partial x} \right) - \bar{B}_{11} \frac{\partial^2 w}{\partial x^2} + 2b\tau_s \\ &\quad - b\tau_s \left(\frac{\partial w}{\partial x} \right)^2 + C^* \left(\tau_s \frac{\partial^2 w}{\partial x^2} - \rho_s \frac{\partial^2 w}{\partial t^2} \right) \\ M_{xx} &= b \int_{-\frac{h}{2}}^{\frac{h}{2}} \sigma_{xx} z dz = B_{11} \left(\frac{1}{2} \left(\frac{\partial w}{\partial x} \right)^2 + \frac{\partial u}{\partial x} \right) - D_{11} \frac{\partial^2 w}{\partial x^2} \\ \bar{M}_{xx} &= \bar{B}_{11} \left(\frac{1}{2} \left(\frac{\partial w}{\partial x} \right)^2 + \frac{\partial u}{\partial x} \right) - \bar{D}_{11} \frac{\partial^2 w}{\partial x^2} + G^* \left(\tau_s \frac{\partial^2 w}{\partial x^2} - \rho_s \frac{\partial^2 w}{\partial t^2} \right) \end{aligned} \quad (15)$$

and

$$\begin{aligned}
 A_{11} &= b \int_{-\frac{h}{2}}^{\frac{h}{2}} \{\lambda(z) + 2\mu(z)\} dz, & \bar{A}_{11} &= 2(\lambda_s + 2\mu_s)b \\
 B_{11} &= b \int_{-\frac{h}{2}}^{\frac{h}{2}} \{\lambda(z) + 2\mu(z)\} z dz, & \bar{B}_{11} &= (\lambda_s + 2\mu_s)bh \\
 D_{11} &= b \int_{-\frac{h}{2}}^{\frac{h}{2}} \{\lambda(z) + 2\mu(z)\} z^2 dz, & \bar{D}_{11} &= (\lambda_s + 2\mu_s) \left(\frac{bh^2}{2} + \frac{h^3}{6} \right) \\
 C^* &= b \int_{-\frac{h}{2}}^{\frac{h}{2}} \left\{ \frac{2v(z)z}{(1-v(z))h} \right\} dz, & G^* &= b \int_{-\frac{h}{2}}^{\frac{h}{2}} \left\{ \frac{2v(z)z^2}{(1-v(z))h} \right\} dz
 \end{aligned} \tag{16}$$

Moreover, the work Π_P done by the external harmonic distributed load f can be expressed in the following form:

$$\Pi_P = \int_x f w dx. \tag{17}$$

In addition, the kinetic energy of the nanobeam including surface free energy effects can be calculated as

$$\begin{aligned}
 \Pi_T &= \frac{1}{2} \int_x \int_s \rho(z) \left\{ \left(\frac{\partial u_x}{\partial t} \right)^2 + \left(\frac{\partial u_z}{\partial t} \right)^2 \right\} dx ds \\
 &+ \frac{1}{2} \left(\int_{S^+} \rho_s \left\{ \left(\frac{\partial u_x}{\partial t} \right)^2 + \left(\frac{\partial u_z}{\partial t} \right)^2 \right\} dS^+ \right. \\
 &\left. + \int_{S^-} \rho_s \left\{ \left(\frac{\partial u_x}{\partial t} \right)^2 + \left(\frac{\partial u_z}{\partial t} \right)^2 \right\} dS^- \right) \\
 &= \frac{1}{2} \int_x \left\{ I_0 \left[\left(\frac{\partial u}{\partial t} \right)^2 + \left(\frac{\partial w}{\partial t} \right)^2 \right] - 2I_1 \frac{\partial u}{\partial t} \frac{\partial^2 w}{\partial x \partial t} + I_2 \left(\frac{\partial^2 w}{\partial x \partial t} \right)^2 \right\} dx,
 \end{aligned} \tag{18}$$

where

$$\begin{aligned}
 zI_0^* &= b \int_{-\frac{h}{2}}^{\frac{h}{2}} \rho(z) dz + 2\rho_s(b+h), \\
 I_1^* &= b \int_{-\frac{h}{2}}^{\frac{h}{2}} \rho(z) z dz + \rho_s \left(bh + \frac{h^2}{2} \right) \\
 I_2^* &= b \int_{-\frac{h}{2}}^{\frac{h}{2}} \rho(z) z^2 dz + \frac{\rho_s(3bh^2 + h^3)}{6}
 \end{aligned} \tag{19}$$

Now, using the Hamilton principle as below

$$\delta \int_{t_1}^{t_2} (\Pi_T - \Pi_s + \Pi_P) dt = 0 \tag{20}$$

it yields

$$\frac{\partial}{\partial x} (N_{xx} + \bar{N}_{xx}) = I_0^* \frac{\partial^2 u}{\partial t^2} - I_1^* \frac{\partial^2 w}{\partial x \partial t}. \tag{21a}$$

$$\begin{aligned}
 \frac{\partial}{\partial x} \left[(N_{xx} + \bar{N}_{xx}) \frac{\partial w}{\partial x} \right] + \frac{\partial^2}{\partial x^2} [M_{xx} + \bar{M}_{xx}] \\
 = f + I_0^* \frac{\partial^2 w}{\partial t^2} - I_2^* \frac{\partial^4 w}{\partial x^2 \partial t^2}.
 \end{aligned} \tag{21b}$$

For the FG porous silicon material, it is assumed that $A_{11}^* = A_{11} + \bar{A}_{11}$, $B_{11}^* = B_{11} + \bar{B}_{11}$, $D_{11}^* = D_{11} + \bar{D}_{11}$. (22)

Therefore, one will have

$$\begin{aligned}
 \frac{\partial u}{\partial x} &= \frac{N_{xx} + \bar{N}_{xx}}{A_{11}^*} + \left(\frac{b\tau_s}{A_{11}^*} - \frac{1}{2} \right) \left(\frac{\partial w}{\partial x} \right)^2 - \frac{2b\tau_s}{A_{11}^*} + \frac{B_{11}^*}{A_{11}^*} \frac{\partial^2 w}{\partial x^2} \\
 &- \frac{C^*}{A_{11}^*} \left(\tau_s \frac{\partial^2 w}{\partial x^2} - \rho_s \frac{\partial^2 w}{\partial t^2} \right).
 \end{aligned} \tag{23}$$

By integrating Eq. (23) and taking immovable end supports into account, it yields

$$\begin{aligned}
 N_{xx} + \bar{N}_{xx} &= 2b\tau_s + \left(\frac{A_{11}^*}{2L} - \frac{b\tau_s}{L} \right) \int_0^L \left(\frac{\partial w}{\partial x} \right)^2 dx - B_{11}^* \frac{\partial^2 w}{\partial x^2} \\
 &+ C^* \left(\tau_s \frac{\partial^2 w}{\partial x^2} - \rho_s \frac{\partial^2 w}{\partial t^2} \right).
 \end{aligned} \tag{24}$$

Substitution Eq. (24) into Eq. (21b) leads to the size-dependent nonlinear governing differential equation of motion for an FG porous nanobeam incorporating surface free energy effects as follows

$$\begin{aligned}
 -D_{11}^* \frac{\partial^4 w}{\partial x^4} + G^* \left(\tau_s \frac{\partial^2 w}{\partial x^2} - \rho_s \frac{\partial^2 w}{\partial t^2} \right) \\
 + \left[\left(\frac{A_{11}^*}{2L} - \frac{b\tau_s}{L} \right) \int_0^L \left(\frac{\partial w}{\partial x} \right)^2 dx + 2b\tau_s - B_{11}^* \frac{\partial^2 w}{\partial x^2} \right. \\
 \left. + C^* \left(\tau_s \frac{\partial^2 w}{\partial x^2} - \rho_s \frac{\partial^2 w}{\partial t^2} \right) \right] \frac{\partial^2 w}{\partial x^2} = f + I_0^* \frac{\partial^2 w}{\partial t^2} - I_2^* \frac{\partial^4 w}{\partial x^2 \partial t^2}.
 \end{aligned} \tag{25}$$

3 Multiple time-scales solving process

To continue the solving process in a more general form, the following dimensionless parameters are introduced:

$$\begin{aligned}
 W &= \frac{w}{h}, \quad X = \frac{x}{L}, \quad \xi = \frac{h}{L}, \quad t = \frac{t}{L} \sqrt{\frac{\lambda_0 + 2\mu_0}{\rho}}, \\
 F &= \frac{fL^2}{(\lambda_0 + 2\mu_0)bh^2} \\
 \{\hat{I}_0, \hat{I}_2\} &= \left\{ \frac{I_0^*}{\rho_0bh}, \frac{I_2^*}{\rho_0bh^3} \right\}, \quad \hat{\tau} = \frac{\tau_s}{(\lambda_0 + 2\mu_0)h}, \quad \hat{\rho} = \frac{\rho_s}{\rho_0h} \\
 \{a_{11}^*, b_{11}^*, d_{11}^*\} &= \left\{ \frac{A_{11}^*}{(\lambda_0 + 2\mu_0)bh}, \frac{B_{11}^*}{(\lambda_0 + 2\mu_0)bh^2}, \frac{D_{11}^*}{(\lambda_0 + 2\mu_0)bh^3} \right\}, \\
 \{c^*, g^*\} &= \left\{ \frac{C^*}{bh}, \frac{G^*}{bh^2} \right\}
 \end{aligned} \tag{26}$$

where λ_0, μ_0 , and ρ_0 are, respectively, the elastic Lamé constants and mass density for the silicon without porosity.

As a result, the dimensionless size-dependent nonlinear governing differential equation of motion takes the following form:

$$\begin{aligned}
 -a_{11}^* \xi^2 \frac{\partial^4 W}{\partial X^4} + g^* \left(\hat{\tau} \xi^2 \frac{\partial^2 W}{\partial X^2} - \hat{\rho} \frac{\partial^2 W}{\partial t^2} \right) \\
 + \left[\frac{(a_{11}^* - 2\hat{\tau}) \xi^2}{2} \int_0^1 \left(\frac{\partial W}{\partial X} \right)^2 dX + 2\hat{\tau} - b_{11}^* \xi^2 \frac{\partial^2 W}{\partial X^2} \right. \\
 \left. + c^* \left(\hat{\tau} \xi^2 \frac{\partial^2 W}{\partial X^2} - \hat{\rho} \frac{\partial^2 W}{\partial t^2} \right) \right] \frac{\partial^2 W}{\partial X^2} = F + \hat{I}_0 \frac{\partial^2 W}{\partial t^2} - \hat{I}_2 \frac{\partial^4 W}{\partial X^2 \partial t^2}.
 \end{aligned} \tag{27}$$

Subsequently, with the aid of the Galerkin method, the solution of the problem can be written in discretized form. To this end, it is assumed that $W(X, t)$ can be expressed as combination of the three first modes as follows:

$$W(X, t) = \sum_{n=1}^3 \varphi_n(X) q_n(t). \tag{28}$$

The analytical expressions for $\varphi_n(X)$ corresponding to different types of boundary conditions are considered based on the linear vibration modes as follows:

- For simply supported–simply supported boundary conditions:

$$\varphi_n(X) = \sin(e_n X), \quad e_n = n\pi. \tag{29}$$

- For clamped–clamped boundary conditions:

$$\begin{aligned}
 \varphi_n(X) &= \cos(e_n X) - \cos h(e_n X) \\
 &+ \left(\frac{\cos(e_n) - \cos h(e_n)}{\sin(e_n) - \sin h(e_n)} \right) (\sin h(e_n X) - \sin(e_n X))
 \end{aligned}$$

$$e_1, e_2, e_3 = 4.7300, 7.8532, 10.9956. \tag{30}$$

- For simply supported–clamped boundary conditions:

$$\begin{aligned}
 \varphi_n(X) &= \cos(e_n X) - \cos h(e_n X) \\
 &+ \left(\frac{\cos(e_n) - \cos h(e_n)}{\sin(e_n) - \sin h(e_n)} \right) (\sin h(e_n X) - \sin(e_n X))
 \end{aligned}$$

$$e_1, e_2, e_3 = 3.9266, 7.0686, 10.2102. \tag{31}$$

- For clamped–free boundary conditions:

$$\begin{aligned}
 \varphi_n(X) &= \cos(e_n X) - \cos h(e_n X) \\
 &+ \left(\frac{\cos(e_n) - \cos h(e_n)}{\sin(e_n) - \sin h(e_n)} \right) (\sin h(e_n X) - \sin(e_n X))
 \end{aligned}$$

$$e_1, e_2, e_3 = 1.8751, 4.6941, 7.8547 \tag{32}$$

In the case of hard excitation, the order of the external distributed load is higher than that of the damping and nonlinear terms. Consequently, by inserting Eq. (28) in the governing differential Eq. (27), one will have

$$\begin{aligned}
 \ddot{q}_1 + \omega_1^2 q_1 + \alpha_1 q_1^3 + \alpha_2 q_2^3 + \alpha_3 q_3^3 + \alpha_4 q_2 q_1^2 + \alpha_5 q_3 q_1^2 \\
 + \alpha_6 q_1 q_2^2 + \alpha_7 q_3 q_2^2 + \alpha_8 q_1 q_3^2 + \alpha_9 q_2 q_3^2 \\
 + \alpha_{10} q_1 q_2 q_3 = 2F \cos(\Omega T)
 \end{aligned} \tag{33a}$$

$$\begin{aligned}
 \ddot{q}_2 + \omega_2^2 q_2 + \beta_1 q_1^3 + \beta_2 q_2^3 + \beta_3 q_3^3 + \beta_4 q_2 q_1^2 \\
 + \beta_5 q_3 q_1^2 + \beta_6 q_1 q_2^2 + \beta_7 q_3 q_2^2 + \beta_8 q_1 q_3^2 + \beta_9 q_2 q_3^2 \\
 + \beta_{10} q_1 q_2 q_3 = 0
 \end{aligned} \tag{33b}$$

$$\begin{aligned}
 \ddot{q}_3 + \omega_3^2 q_3 + \gamma_1 q_1^3 + \gamma_2 q_2^3 + \gamma_3 q_3^3 + \gamma_4 q_2 q_1^2 + \gamma_5 q_3 q_1^2 \\
 + \gamma_6 q_1 q_2^2 + \gamma_7 q_3 q_2^2 + \gamma_8 q_1 q_3^2 + \gamma_9 q_2 q_3^2 \\
 + \gamma_{10} q_1 q_2 q_3 = 0.
 \end{aligned} \tag{33c}$$

To continue the solution methodology, it is assumed that the external distributed load is a dissipative one, so the damping parameter can be defined as

$$\vartheta = \frac{\mathcal{G} \omega_1^2}{\omega_L}, \tag{34}$$

in which ω_L stands for the linear frequency of the system, and \mathcal{G} is a constant.

Furthermore, it is assumed that $\hat{t} = \hat{\omega}_1 t$, and $\hat{q}_i = \epsilon q_i$, $i = 1, 2, 3$, where $\hat{\omega}_1$ represents the first frequency of the FG porous nanobeam in the absence of the surface stress effect. Therefore, scaling Eq. (33) and consideration of the hard excitation yield

$$\ddot{q}_1 + \left(\frac{2\epsilon^2\vartheta}{\hat{\omega}_1}\right)\dot{q}_1 + \left(\frac{\omega_1^2}{\hat{\omega}_1^2}\right)\bar{q}_1 + \left(\frac{\epsilon^2}{\hat{\omega}_1^2}\right)(\alpha_1\bar{q}_1^3 + \alpha_2\bar{q}_2^3 + \alpha_3\bar{q}_3^3 + \alpha_4\bar{q}_2\bar{q}_1^2 + \alpha_5\bar{q}_3\bar{q}_1^2 + \alpha_6\bar{q}_1\bar{q}_2^2 + \alpha_7\bar{q}_3\bar{q}_2^2 + \alpha_8\bar{q}_1\bar{q}_3^2 + \alpha_9\bar{q}_2\bar{q}_3^2 + \alpha_{10}\bar{q}_1\bar{q}_2\bar{q}_3) = \frac{2\epsilon^2 F}{\hat{\omega}_1^2} \cos\left(\frac{\Omega t}{\hat{\omega}_1}\right) \tag{35a}$$

$$O(\epsilon^0) : \begin{cases} \mathcal{D}_0^2 Q_{10} + \left(\frac{\omega_1^2}{\hat{\omega}_1^2}\right) Q_{10} = \frac{2F}{\hat{\omega}_1^2} \cos\left(\frac{\Omega t}{\hat{\omega}_1}\right) \\ \mathcal{D}_0^2 Q_{20} + \left(\frac{\omega_2^2}{\hat{\omega}_1^2}\right) Q_{20} = 0 \\ \mathcal{D}_0^2 Q_{30} + \left(\frac{\omega_3^2}{\hat{\omega}_1^2}\right) Q_{30} = 0 \end{cases} \tag{37}$$

$$O(\epsilon^2) : \begin{cases} \mathcal{D}_0^2 Q_{12} + \left(\frac{\omega_1^2}{\hat{\omega}_1^2}\right) Q_{12} = -2\mathcal{D}_0\mathcal{D}_2 Q_{10} - \left(\frac{2\vartheta}{\hat{\omega}_1}\right)\mathcal{D}_0 Q_{10} - \left(\frac{\alpha_1}{\hat{\omega}_1^2}\right) Q_{10}^3 - \dots - \left(\frac{\alpha_1}{\hat{\omega}_1^2}\right) Q_{10} Q_{20} Q_{30} \\ \mathcal{D}_0^2 Q_{22} + \left(\frac{\omega_2^2}{\hat{\omega}_1^2}\right) Q_{22} = -2\mathcal{D}_0\mathcal{D}_2 Q_{20} - \left(\frac{2\vartheta}{\hat{\omega}_1}\right)\mathcal{D}_0 Q_{20} - \left(\frac{\alpha_1}{\hat{\omega}_1^2}\right) Q_{10}^3 - \dots - \left(\frac{\alpha_1}{\hat{\omega}_1^2}\right) Q_{10} Q_{20} Q_{30} \\ \mathcal{D}_0^2 Q_{32} + \left(\frac{\omega_3^2}{\hat{\omega}_1^2}\right) Q_{32} = -2\mathcal{D}_0\mathcal{D}_2 Q_{30} - \left(\frac{2\vartheta}{\hat{\omega}_1}\right)\mathcal{D}_0 Q_{30} - \left(\frac{\alpha_1}{\hat{\omega}_1^2}\right) Q_{10}^3 - \dots - \left(\frac{\alpha_1}{\hat{\omega}_1^2}\right) Q_{10} Q_{20} Q_{30} \end{cases} \tag{38}$$

$$\ddot{q}_2 + \left(\frac{2\epsilon^2\vartheta}{\hat{\omega}_1}\right)\dot{q}_2 + \left(\frac{\omega_2^2}{\hat{\omega}_1^2}\right)\bar{q}_2 + \left(\frac{\epsilon^2}{\hat{\omega}_1^2}\right)(\alpha_1\bar{q}_1^3 + \alpha_2\bar{q}_2^3 + \alpha_3\bar{q}_3^3 + \alpha_4\bar{q}_2\bar{q}_1^2 + \alpha_5\bar{q}_3\bar{q}_1^2 + \alpha_6\bar{q}_1\bar{q}_2^2 + \alpha_7\bar{q}_3\bar{q}_2^2 + \alpha_8\bar{q}_1\bar{q}_3^2 + \alpha_9\bar{q}_2\bar{q}_3^2 + \alpha_{10}\bar{q}_1\bar{q}_2\bar{q}_3) = 0 \tag{35b}$$

$$\ddot{q}_3 + \left(\frac{2\epsilon^2\vartheta}{\hat{\omega}_1}\right)\dot{q}_3 + \left(\frac{\omega_3^2}{\hat{\omega}_1^2}\right)\bar{q}_3 + \left(\frac{\epsilon^2}{\hat{\omega}_1^2}\right)(\alpha_1\bar{q}_1^3 + \alpha_2\bar{q}_2^3 + \alpha_3\bar{q}_3^3 + \alpha_4\bar{q}_2\bar{q}_1^2 + \alpha_5\bar{q}_3\bar{q}_1^2 + \alpha_6\bar{q}_1\bar{q}_2^2 + \alpha_7\bar{q}_3\bar{q}_2^2 + \alpha_8\bar{q}_1\bar{q}_3^2 + \alpha_9\bar{q}_2\bar{q}_3^2 + \alpha_{10}\bar{q}_1\bar{q}_2\bar{q}_3) = 0. \tag{35c}$$

Thereafter, the following multiple time-scales summations are taken into account for $\bar{q}_i (i = 1, 2, 3)$:

$$\bar{q}_1(\hat{t}, \epsilon) = Q_{10}(T_0, T_1, T_2) + \epsilon Q_{11}(T_0, T_1, T_2) + \epsilon^2 Q_{12}(T_0, T_1, T_2) \tag{36a}$$

$$\bar{q}_2(\hat{t}, \epsilon) = Q_{20}(T_0, T_1, T_2) + \epsilon Q_{21}(T_0, T_1, T_2) + \epsilon^2 Q_{22}(T_0, T_1, T_2) \tag{36b}$$

$$\bar{q}_3(\hat{t}, \epsilon) = Q_{30}(T_0, T_1, T_2) + \epsilon Q_{31}(T_0, T_1, T_2) + \epsilon^2 Q_{32}(T_0, T_1, T_2), \tag{36c}$$

where $T_0 = \hat{t}$, $T_1 = \epsilon\hat{t}$, and $T_2 = \epsilon^2\hat{t}$. After substitution Eq. (36) into Eq. (35), it is seen that the solution of the problem is not dependent on T_1 . Therefore, one will have

in which $\mathcal{D}_i^j = \frac{d^j}{dt_i^j}$ denote the time derivatives.

Now, the following parameters are introduced:

$$\tilde{F} = \frac{F}{\hat{\omega}_1^2}, \quad \tilde{\Omega} = \frac{\Omega}{\hat{\omega}_1}, \quad \left\{ \begin{matrix} \tilde{\alpha}_i, \tilde{\beta}_i, \tilde{\gamma}_i \\ \tilde{\omega}_1, \tilde{\omega}_2, \tilde{\omega}_3 \end{matrix} \right\} = \left\{ \begin{matrix} \frac{\alpha_i}{\hat{\omega}_1^2}, \frac{\beta_i}{\hat{\omega}_1^2}, \frac{\gamma_i}{\hat{\omega}_1^2} \\ \frac{\omega_1}{\hat{\omega}_1}, \frac{\omega_2}{\hat{\omega}_1}, \frac{\omega_3}{\hat{\omega}_1} \end{matrix} \right\} \tag{39}$$

$i = 1, 2, \dots, 10$

On the basis of the Eq. (37), it can be written

$$\begin{aligned} Q_{10} &= \mathcal{A}(T_1, T_2)e^{i\tilde{\omega}_1 T_0} + \Delta e^{i\tilde{\Omega} T_0} + CC \\ Q_{20} &= \mathcal{B}(T_1, T_2)e^{i\tilde{\omega}_2 T_0} + CC \\ Q_{30} &= \mathcal{C}(T_1, T_2)e^{i\tilde{\omega}_3 T_0} + CC \end{aligned} \tag{40}$$

in which CC denotes the complex conjugate part of the expression, and

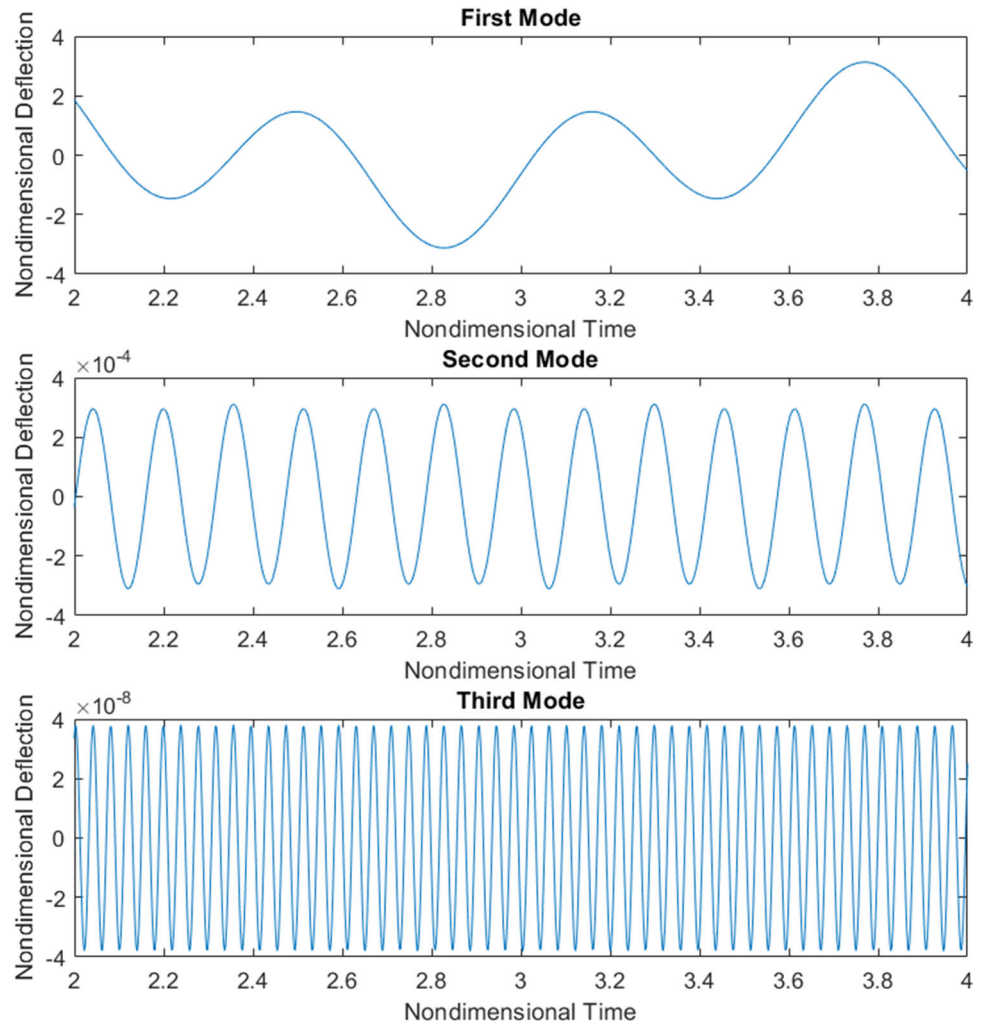
$$\Delta = \frac{\tilde{F}}{\tilde{\omega}_1^2 - \tilde{\Omega}^2}. \tag{41}$$

Thereby, after inserting Eq. (40) in Eq. (38), and performing some mathematical calculations, the secular terms associated with each type of the external excitation are extracted.

3.1 Superharmonic excitation

In accordance with the superharmonic excitation, one can write

Fig. 2 Variation of the oscillation amplitude with time for an FG porous silicon nanobeam under superharmonic excitation corresponding to different mode numbers ($h = 2 \text{ nm}, h/L = 20$, pattern A)



$$3\tilde{\Omega} = \tilde{\omega}_1 + \epsilon\Gamma, \tag{42}$$

where Γ is the detuning parameter. By setting the secular as well as small divisor terms equal to zero, one will have

$$\begin{aligned} & -2i\tilde{\omega}_1 \frac{\partial \mathcal{A}}{\partial T_2} e^{i\tilde{\omega}_1 T_0} - 2i\vartheta\tilde{\omega}_1 \mathcal{A} e^{i\tilde{\omega}_1 T_0} - 3\tilde{\alpha}_1 \mathcal{A}^2 \bar{\mathcal{A}} e^{i\tilde{\omega}_1 T_0} \\ & - 6\tilde{\alpha}_1 \mathcal{A} \Delta^2 e^{i\tilde{\omega}_1 T_0} - \tilde{\alpha}_1 \Delta^3 e^{3i\tilde{\omega}_1 T_0} - 2\tilde{\alpha}_6 \mathcal{A} \mathcal{B} \bar{\mathcal{B}} e^{i\tilde{\omega}_1 T_0} \\ & - 2\tilde{\alpha}_8 \mathcal{A} \mathcal{C} \bar{\mathcal{C}} e^{i\tilde{\omega}_1 T_0} = 0 \end{aligned} \tag{43a}$$

$$\begin{aligned} & -2i\tilde{\omega}_2 \frac{\partial \mathcal{B}}{\partial T_2} e^{i\tilde{\omega}_2 T_0} - 2i\vartheta\tilde{\omega}_2 \mathcal{B} e^{i\tilde{\omega}_2 T_0} - 3\tilde{\beta}_2 \mathcal{B}^2 \bar{\mathcal{B}} e^{i\tilde{\omega}_2 T_0} \\ & - 2\tilde{\beta}_4 \mathcal{B} \Delta^2 e^{i\tilde{\omega}_2 T_0} - 2\tilde{\beta}_4 \mathcal{A} \bar{\mathcal{A}} \mathcal{B} e^{i\tilde{\omega}_2 T_0} - 2\tilde{\beta}_9 \mathcal{B} \mathcal{C} \bar{\mathcal{C}} e^{i\tilde{\omega}_2 T_0} = 0 \end{aligned} \tag{43b}$$

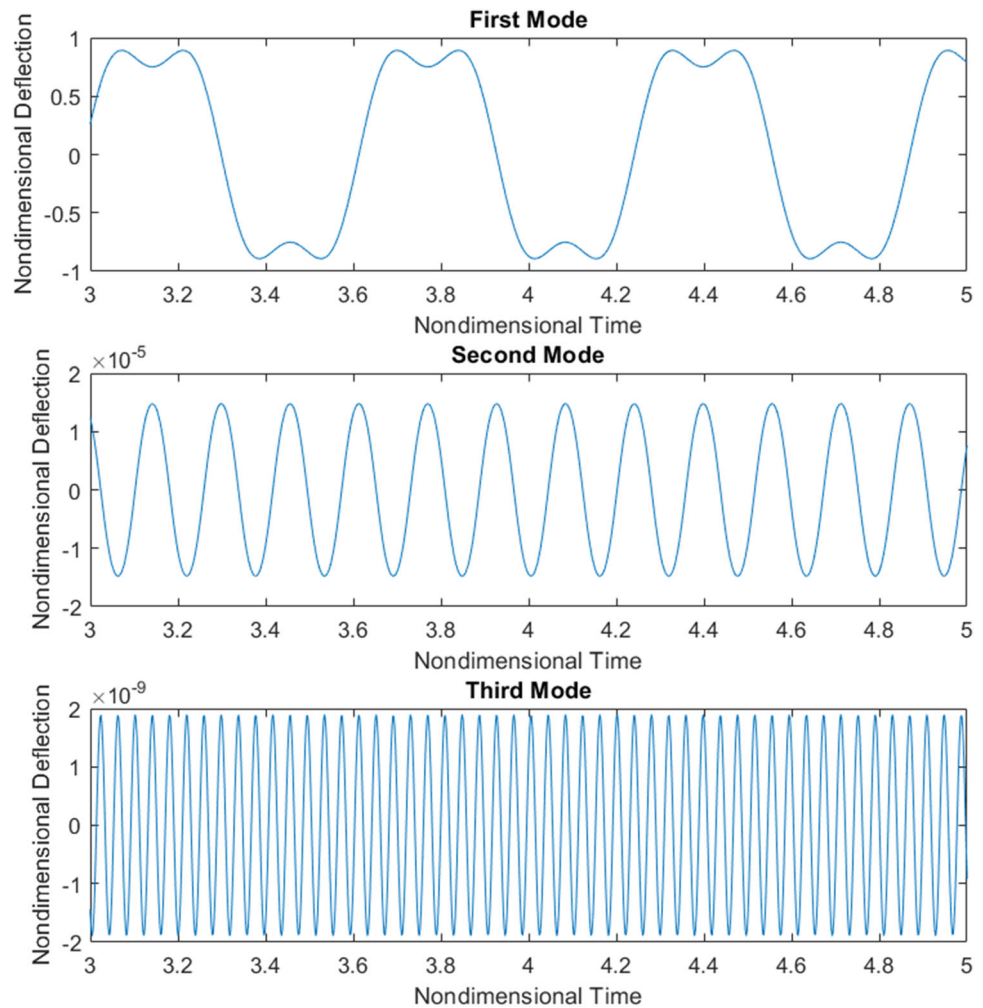
$$\begin{aligned} & -2i\tilde{\omega}_3 \frac{\partial \mathcal{C}}{\partial T_2} e^{i\tilde{\omega}_3 T_0} - 2i\vartheta\tilde{\omega}_3 \mathcal{C} e^{i\tilde{\omega}_3 T_0} - 3\tilde{\gamma}_3 \mathcal{C}^2 \bar{\mathcal{C}} e^{i\tilde{\omega}_3 T_0} \\ & - 2\tilde{\gamma}_5 \mathcal{C} \Delta^2 e^{i\tilde{\omega}_3 T_0} \\ & - 2\tilde{\gamma}_5 \mathcal{A} \bar{\mathcal{A}} \mathcal{C} e^{i\tilde{\omega}_3 T_0} - 2\tilde{\gamma}_7 \mathcal{C} \mathcal{B} \bar{\mathcal{B}} e^{i\tilde{\omega}_3 T_0} = 0 \end{aligned} \tag{43c}$$

Now, $\mathcal{A}(T_1, T_2), \mathcal{B}(T_1, T_2)$ and $\mathcal{C}(T_1, T_2)$ are considered in polar function form as below:

$$\begin{aligned} \mathcal{A}(T_1, T_2) &= \frac{1}{2} a(T_1, T_2) e^{i\psi(T_1, T_2)} \\ \mathcal{B}(T_1, T_2) &= \frac{1}{2} \ell(T_1, T_2) e^{i\eta(T_1, T_2)} \\ \mathcal{C}(T_1, T_2) &= \frac{1}{2} c(T_1, T_2) e^{i\psi(T_1, T_2)} \end{aligned} \tag{44}$$

Inserting Eq. (44) in Eq. (43) leads to the following equations corresponding to each of the real and imaginary parts:

Fig. 3 Variation of the oscillation amplitude with time for an FG porous silicon nanobeam under subharmonic excitation corresponding to different mode numbers ($h = 2 \text{ nm}, h/L = 20$, pattern A)



$$\begin{cases} \frac{da}{dT_2} = -\vartheta a - \frac{\tilde{\alpha}_1 \Delta^3}{\tilde{\omega}_1} \sin(\Gamma T_2 - \varsigma) \\ a \frac{d\varsigma}{dT_2} = \frac{3\tilde{\alpha}_1}{8\tilde{\omega}_1} a^3 + \frac{3\tilde{\alpha}_1 \Delta^2}{\tilde{\omega}_1} a + \frac{\tilde{\alpha}_1 \Delta^3}{\tilde{\omega}_1} \cos(\Gamma T_2 - \varsigma) \end{cases} \quad (45a)$$

$$\begin{cases} \frac{d\ell}{dT_2} = -\vartheta \ell \\ \ell \frac{d\eta}{dT_2} = \frac{3\tilde{\beta}_2}{8\tilde{\omega}_2} \ell^3 + \frac{\tilde{\beta}_4 \Delta^2}{\tilde{\omega}_2} \ell + \frac{\tilde{\beta}_4 a^2}{4\tilde{\omega}_2} \ell + \frac{\tilde{\beta}_9 c^2}{4\tilde{\omega}_2} \ell \end{cases} \quad (45b)$$

$$\begin{cases} \frac{dc}{dT_2} = -\vartheta c \\ c \frac{d\psi}{dT_2} = \frac{3\tilde{\gamma}_3}{8\tilde{\omega}_3} c^3 + \frac{\tilde{\gamma}_5 \Delta^2}{\tilde{\omega}_3} c + \frac{\tilde{\gamma}_5 a^2}{4\tilde{\omega}_3} c + \frac{\tilde{\gamma}_7 \ell^2}{4\tilde{\omega}_3} c \end{cases} \quad (45c)$$

The oscillation amplitudes of a silicon nanobeam under superharmonic excitation are shown in Fig. 2 corresponding to the first three vibration modes. As it can be observed, the vibration amplitude of the first mode is so higher than those of the second and third modes. As a result, the values of ℓ and c are so small in comparison with the value of a , so it is possible to neglect them. Therefore, Eq. (45) reduces in the following form:

$$\begin{cases} \frac{da}{dT_2} = -\vartheta a - \frac{\tilde{\alpha}_1 \Delta^3}{\tilde{\omega}_1} \sin(\Gamma T_2 - \varsigma) \\ a \frac{d\varsigma}{dT_2} = \frac{3\tilde{\alpha}_1}{8\tilde{\omega}_1} a^3 + \frac{3\tilde{\alpha}_1 \Delta^2}{\tilde{\omega}_1} a + \frac{\tilde{\alpha}_1 \Delta^3}{\tilde{\omega}_1} \cos(\Gamma T_2 - \varsigma) \end{cases} \quad (46)$$

Table 1 Material properties of the silicon material [73, 74]

E (GPa)	210
ν	0.24
μ_s (N/m)	- 2.774
λ_s (N/m)	- 4.488
τ_s (N/m)	0.6048

Table 2 Comparison between the dimensionless natural frequencies of silicon nanobeams with different thicknesses in the presence of the surface stress effect

Thickness (nm)	SS boundary conditions		CC boundary conditions	
	Present study	Ref. [75]	Present study	Ref. [75]
1	0.1828	0.1830	0.2519	0.2524
2	0.1554	0.1557	0.2320	0.2323
5	0.1251	0.1255	0.2114	0.2117
50	0.0935	0.0937	0.1924	0.1928

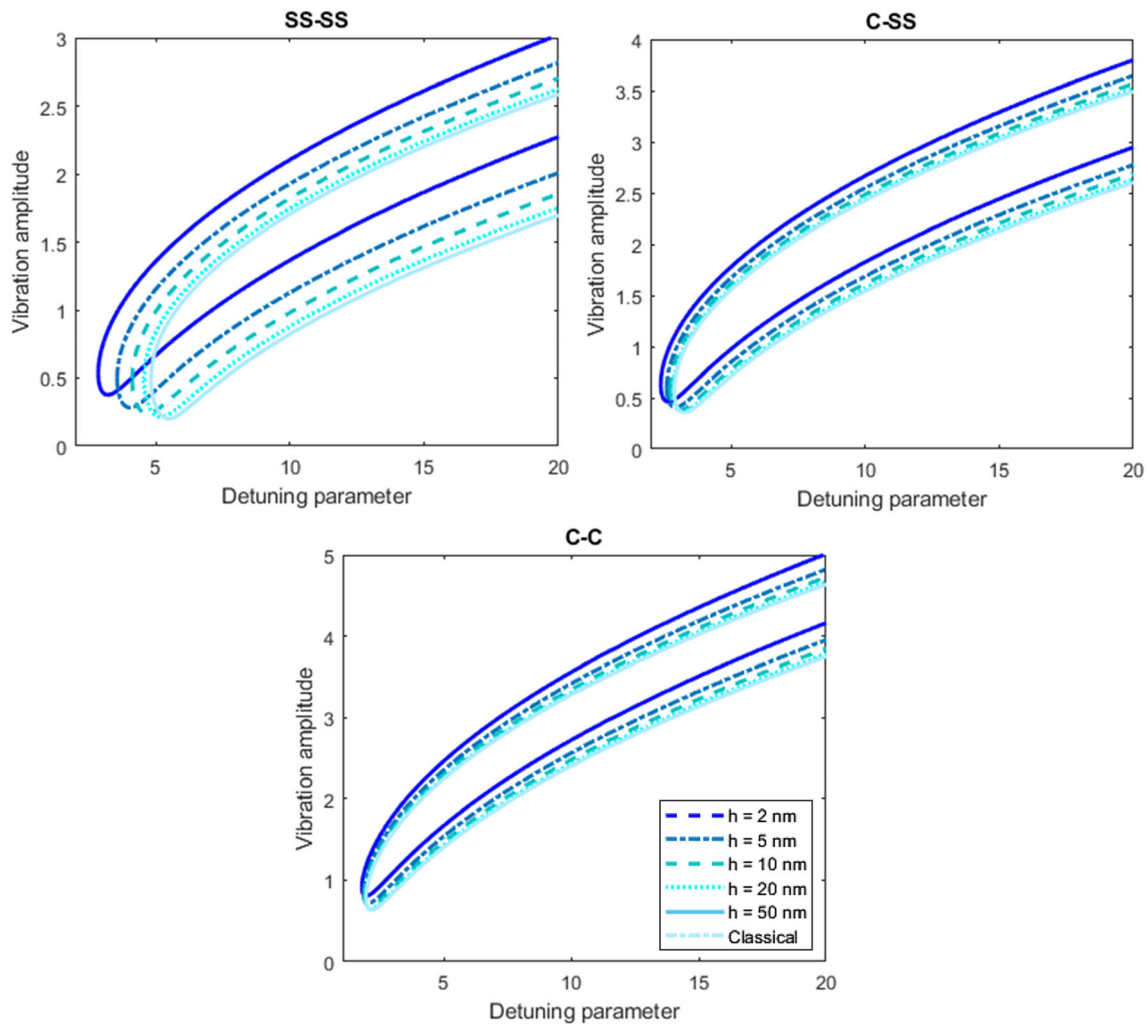


Fig. 4 Frequency response of FG porous silicon nanobeams with different thicknesses under subharmonic excitation based on the classical and surface elastic beam models ($\Gamma_p = 0.4$, pattern A, $\tilde{F} = 0.4$)

The purpose is now to obtain the steady-state solution, so the derivative terms on the left side of Eq. (46) are set to zero. As a result, it gives

$$\left[\vartheta^2 + \left(\Gamma - \frac{3\tilde{\alpha}_1\Delta^2}{\tilde{\omega}_1} - \frac{3\tilde{\alpha}_1a^2}{8\tilde{\omega}_1} \right)^2 \right] a^2 = \frac{\tilde{\alpha}_1^2\Delta^6}{\tilde{\omega}_1^2}. \tag{47}$$

Therefore, the size-dependent frequency response for an FG porous silicon nanobeam under superharmonic excitation can be expressed as

$$\Gamma = \frac{3\tilde{\alpha}_1\Delta^2}{\tilde{\omega}_1} + \frac{3\tilde{\alpha}_1a^2}{8\tilde{\omega}_1} \pm \sqrt{\frac{\tilde{\alpha}_1^2\Delta^6}{a^2\tilde{\omega}_1^2} - \vartheta^2}. \tag{48}$$

On the other hand, Eq. (47) can be rewritten as

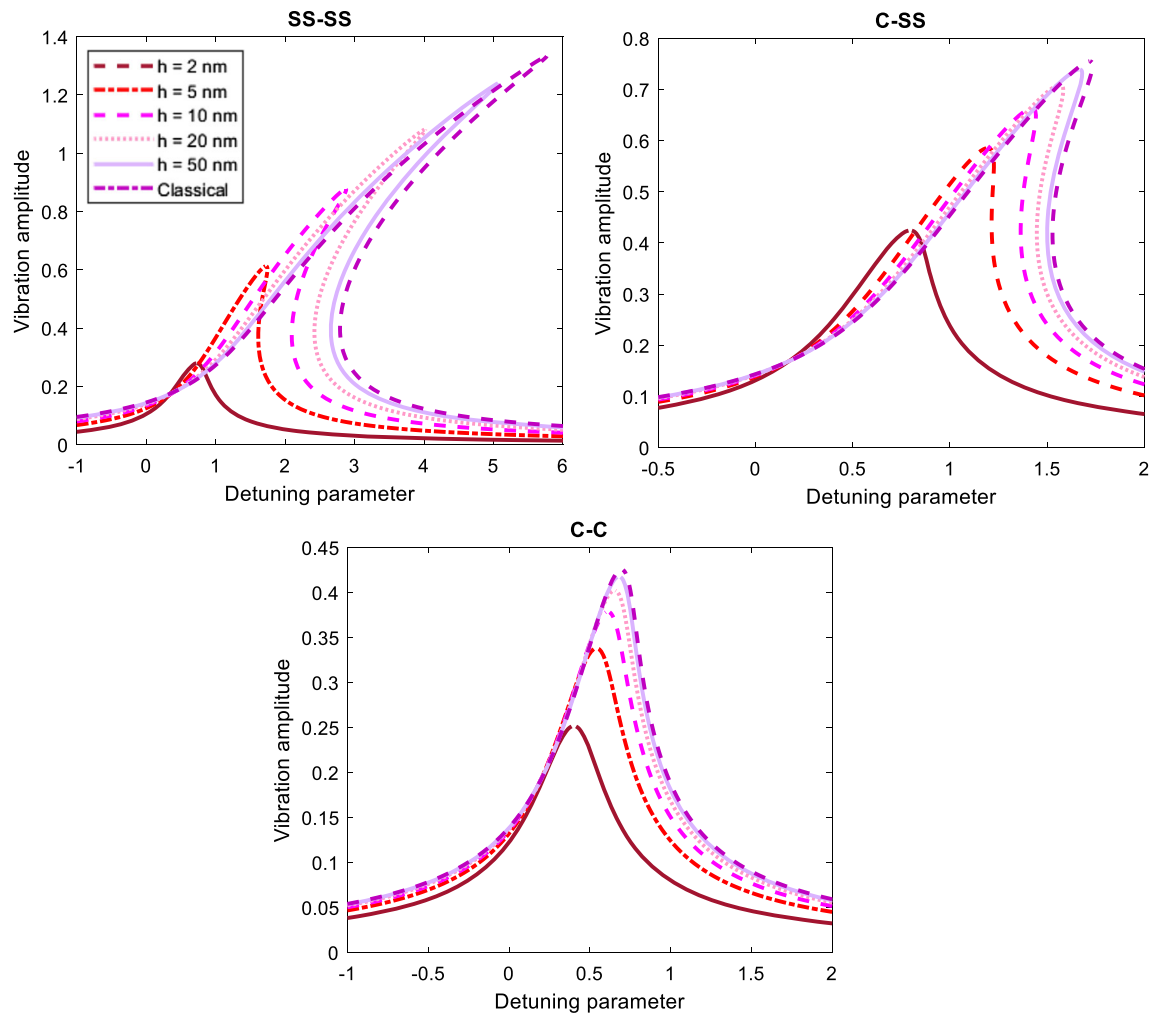


Fig. 5 Frequency response of FG porous silicon nanobeams with different thicknesses under superharmonic excitation based on the classical and surface elastic beam models ($\Gamma_p = 0.4$, pattern A, $\bar{F} = 0.4$)

$$\left(\vartheta^2 + \Gamma^2 + \frac{9\tilde{\alpha}_1^2 \Delta^4}{\tilde{\omega}_1^2} + \frac{9\tilde{\alpha}_1^2 a^4}{64\tilde{\omega}_1^2} - \frac{6\tilde{\alpha}_1 \Delta^2 \Gamma}{\tilde{\omega}_1} - \frac{3\tilde{\alpha}_1 a^2 \Gamma}{4\tilde{\omega}_1} + \frac{9\tilde{\alpha}_1^2 a^2 \Delta^2}{4\tilde{\omega}_1^2} \right) a^2 = \frac{\tilde{\alpha}_1^2 \Delta^6}{\tilde{\omega}_1^2}. \tag{49}$$

Thereby, it yields

$$\mathcal{S}_1 \Delta^6 + \mathcal{S}_2 \Delta^4 + \mathcal{S}_3 \Delta^2 + \mathcal{S}_4 = 0, \tag{50}$$

in which

$$\begin{aligned} \mathcal{S}_1 &= \frac{\tilde{\alpha}_1^2}{\tilde{\omega}_1^2}, & \mathcal{S}_2 &= -\frac{9\tilde{\alpha}_1^2 a^2}{\tilde{\omega}_1^2}, & \mathcal{S}_3 &= \frac{6\tilde{\alpha}_1 \Gamma a^2}{\tilde{\omega}_1} - \frac{9\tilde{\alpha}_1^2 a^4}{4\tilde{\omega}_1^2} \\ \mathcal{S}_4 &= -\left(\vartheta^2 + \Gamma^2 + \frac{9\tilde{\alpha}_1^2 a^4}{64\tilde{\omega}_1^2} - \frac{3\tilde{\alpha}_1 a^2 \Gamma}{4\tilde{\omega}_1} \right) a^2. \end{aligned} \tag{51}$$

The solution of Eq. (50) results in the size-dependent amplitude response of an FG porous silicon nanobeam under superharmonic excitation in the presence of surface stress effect.

3.2 Subharmonic excitation

In accordance with the subharmonic excitation, one can write

$$\tilde{\Omega} = 3\tilde{\omega}_1 + \epsilon\Gamma. \tag{52}$$

Afterwards, by eliminating the secular and small divisor terms, the following sets of equations can be obtained:

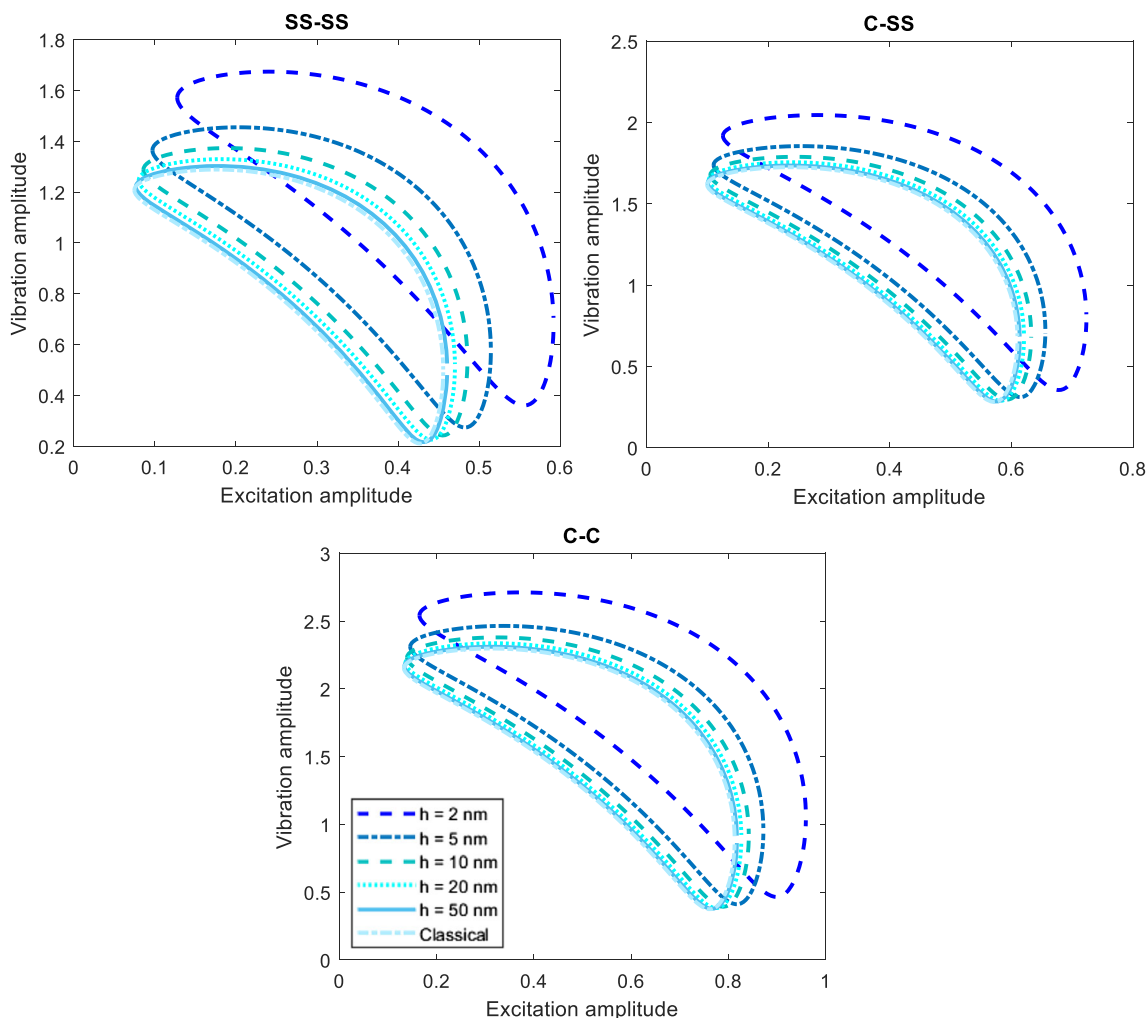


Fig. 6 Amplitude response of FG porous silicon nanobeams with different thicknesses under subharmonic excitation based on the classical and surface elastic beam models ($\Gamma_p = 0.4$, pattern A, $\Gamma = 5$)

$$\begin{aligned}
 & -2i\tilde{\omega}_1 \frac{\partial \mathcal{A}}{\partial T_2} e^{i\tilde{\omega}_1 T_0} - 2i\vartheta \tilde{\omega}_1 \mathcal{A} e^{i\tilde{\omega}_1 T_0} - 3\tilde{\alpha}_1 \mathcal{A}^2 \bar{\mathcal{A}} e^{i\tilde{\omega}_1 T_0} \\
 & - 6\tilde{\alpha}_1 \mathcal{A} \Delta^2 e^{i\tilde{\omega}_1 T_0} - 3\tilde{\alpha}_1 \mathcal{A}^2 \Delta e^{i(\tilde{\omega}-2\tilde{\omega}_1)T_0} \\
 & - 2\tilde{\alpha}_6 \mathcal{A} \mathcal{B} \bar{\mathcal{B}} e^{i\tilde{\omega}_1 T_0} - 2\tilde{\alpha}_8 \mathcal{A} \mathcal{C} \bar{\mathcal{C}} e^{i\tilde{\omega}_1 T_0} = 0
 \end{aligned} \tag{53a}$$

$$\begin{aligned}
 & -2i\tilde{\omega}_2 \frac{\partial \mathcal{B}}{\partial T_2} e^{i\tilde{\omega}_2 T_0} - 2i\vartheta \tilde{\omega}_2 \mathcal{B} e^{i\tilde{\omega}_2 T_0} - 3\tilde{\beta}_2 \mathcal{B}^2 \bar{\mathcal{B}} e^{i\tilde{\omega}_2 T_0} \\
 & - 2\tilde{\beta}_4 \mathcal{B} \Delta^2 e^{i\tilde{\omega}_2 T_0} - 2\tilde{\beta}_4 \mathcal{A} \bar{\mathcal{A}} \mathcal{B} e^{i\tilde{\omega}_2 T_0} - 2\tilde{\beta}_9 \mathcal{B} \mathcal{C} \bar{\mathcal{C}} e^{i\tilde{\omega}_2 T_0} = 0
 \end{aligned} \tag{53b}$$

$$\begin{aligned}
 & -2i\tilde{\omega}_3 \frac{\partial \mathcal{C}}{\partial T_2} e^{i\tilde{\omega}_3 T_0} - 2i\vartheta \tilde{\omega}_3 \mathcal{C} e^{i\tilde{\omega}_3 T_0} - 3\tilde{\gamma}_3 \mathcal{C}^2 \bar{\mathcal{C}} e^{i\tilde{\omega}_3 T_0} \\
 & - 2\tilde{\gamma}_5 \mathcal{C} \Delta^2 e^{i\tilde{\omega}_3 T_0} - 2\tilde{\gamma}_5 \mathcal{A} \bar{\mathcal{A}} \mathcal{C} e^{i\tilde{\omega}_3 T_0} - 2\tilde{\gamma}_7 \mathcal{C} \mathcal{B} \bar{\mathcal{B}} e^{i\tilde{\omega}_3 T_0} = 0.
 \end{aligned} \tag{53c}$$

$$\begin{cases} \frac{da}{dT_2} = -\vartheta a - \frac{3\tilde{\alpha}_1 a^2 \Delta}{4\tilde{\omega}_1} \sin(\Gamma T_2 - 3\zeta) \\ a \frac{d\zeta}{dT_2} = \frac{3\tilde{\alpha}_1}{8\tilde{\omega}_1} a^3 + \frac{3\tilde{\alpha}_1 \Delta^2}{\tilde{\omega}_1} a + \frac{3\tilde{\alpha}_1 a^2 \Delta}{4\tilde{\omega}_1} \cos(\Gamma T_2 - 3\zeta) \end{cases} \tag{54a}$$

$$\begin{cases} \frac{d\ell}{dT_2} = -\vartheta \ell \\ \ell \frac{d\eta}{dT_2} = \frac{3\tilde{\beta}_2}{8\tilde{\omega}_2} \ell^3 + \frac{\tilde{\beta}_4 \Delta^2}{\tilde{\omega}_2} \ell + \frac{\tilde{\beta}_4 a^2}{4\tilde{\omega}_2} \ell + \frac{\tilde{\beta}_9 c^2}{4\tilde{\omega}_2} \ell \end{cases} \tag{54b}$$

$$\begin{cases} \frac{dc}{dT_2} = -\vartheta c \\ c \frac{d\psi}{dT_2} = \frac{3\tilde{\gamma}_3}{8\tilde{\omega}_3} c^3 + \frac{\tilde{\gamma}_5 \Delta^2}{\tilde{\omega}_3} c + \frac{\tilde{\gamma}_5 a^2}{4\tilde{\omega}_3} c + \frac{\tilde{\gamma}_7 \ell^2}{4\tilde{\omega}_3} c \end{cases} \tag{54c}$$

For $\mathcal{A}(T_1, T_2)$, $\mathcal{B}(T_1, T_2)$ and $\mathcal{C}(T_1, T_2)$, a polar function is assumed similar to Eq. (47), so one will have

The oscillation amplitudes of an FG porous silicon nanobeam subjected to subharmonic excitation are illustrated in Fig. 3 corresponding to the first three vibration

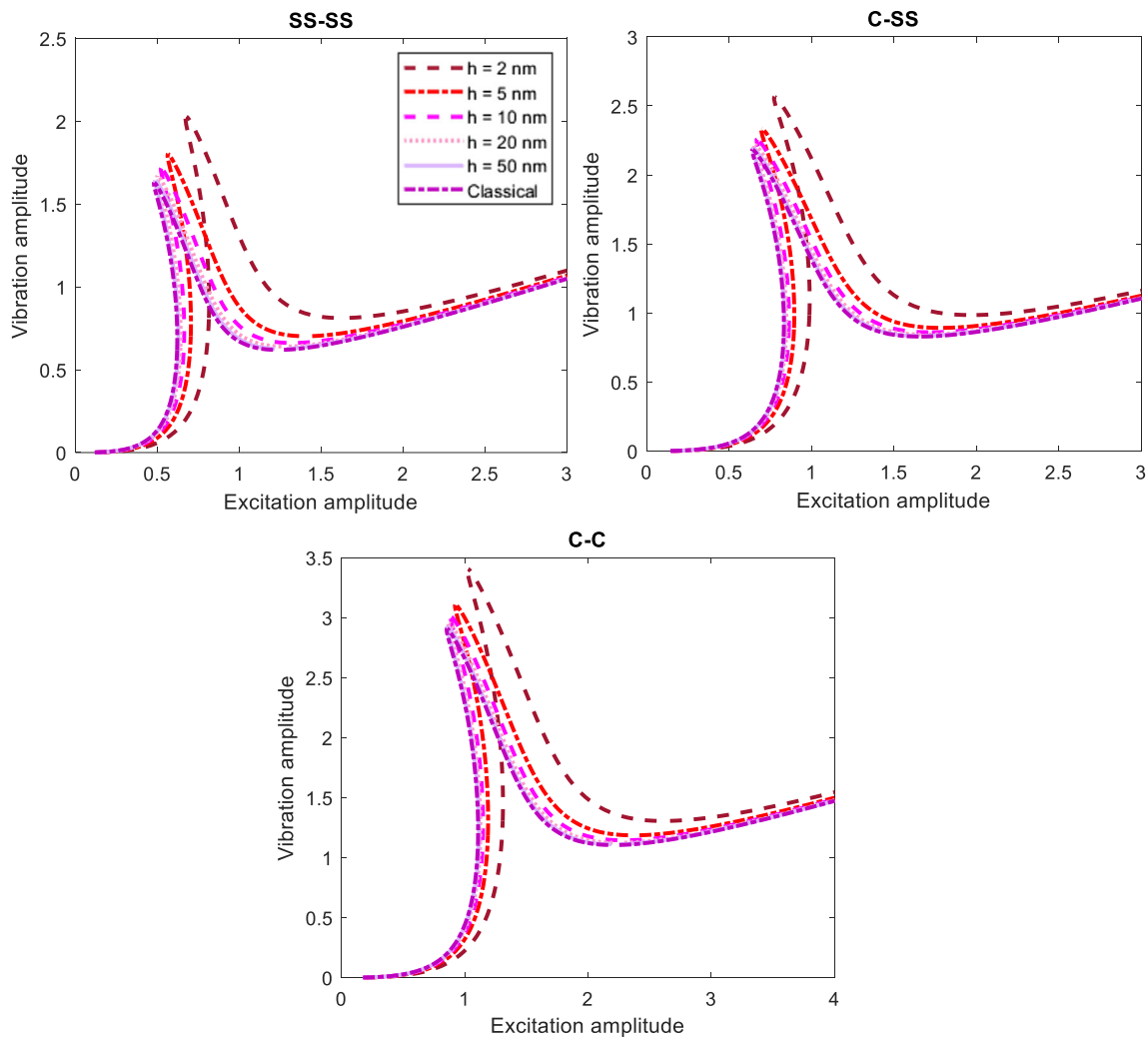


Fig. 7 Amplitude response of FG porous silicon nanobeams with different thicknesses under superharmonic excitation based on the classical and surface elastic beam models ($\Gamma_p = 0.4$, pattern A, $\Gamma = 5$)

modes. It is obvious that the oscillation amplitude of the first mode is so higher than those of the second and third modes. As a result, the values of ℓ and c are so small in comparison with the value of a , so it is possible to neglect them. Therefore, Eq. (54) reduces to the following form

$$\begin{cases} \frac{da}{dT_2} = -\vartheta a - \frac{3\tilde{\alpha}_1 a^2 \Delta}{4\tilde{\omega}_1} \sin(\Gamma T_2 - 3\zeta) \\ a \frac{d\zeta}{dT_2} = \frac{3\tilde{\alpha}_1}{8\tilde{\omega}_1} a^3 + \frac{3\tilde{\alpha}_1 \Delta^2}{\tilde{\omega}_1} a + \frac{3\tilde{\alpha}_1 a^2 \Delta}{4\tilde{\omega}_1} \cos(\Gamma T_2 - 3\zeta) \end{cases} \quad (55)$$

The purpose is now to obtain the steady-state solution, so the derivative terms on the left side of Eq. (55) are set to zero. As a result, it gives

$$9\vartheta^2 + \left(\Gamma - \frac{9\tilde{\alpha}_1 \Delta^2}{\tilde{\omega}_1} - \frac{9\tilde{\alpha}_1 a^2}{8\tilde{\omega}_1} \right)^2 = \frac{81\tilde{\alpha}_1^2 a^2 \Delta^2}{16\tilde{\omega}_1^2}. \quad (56)$$

Consequently, the frequency response for an FG porous silicon nanobeam under subharmonic excitation and in the presence of surface free energy effect can be written as

$$\Gamma = \frac{9\tilde{\alpha}_1 \Delta^2}{\tilde{\omega}_1} + \frac{9\tilde{\alpha}_1 a^2}{8\tilde{\omega}_1} \pm \sqrt{\frac{81\tilde{\alpha}_1^2 a^2 \Delta^2}{16\tilde{\omega}_1^2} - 9\vartheta^2}. \quad (57)$$

On the other hand, Eq. (56) can be rewritten as

$$\begin{aligned} & \left(9\vartheta^2 + \Gamma^2 + \frac{81\tilde{\alpha}_1^2 \Delta^4}{\tilde{\omega}_1^2} + \frac{81\tilde{\alpha}_1^2 a^4}{64\tilde{\omega}_1^2} - \frac{18\tilde{\alpha}_1 \Delta^2 \Gamma}{\tilde{\omega}_1} - \frac{9\tilde{\alpha}_1 a^2 \Gamma}{4\tilde{\omega}_1} + \frac{81\tilde{\alpha}_1^2 a^2 \Delta^2}{4\tilde{\omega}_1^2} \right) \\ & = \frac{81\tilde{\alpha}_1^2 a^2 \Delta^2}{16\tilde{\omega}_1^2}. \end{aligned} \quad (58)$$

Therefore, it yields

$$\mu_1 \Delta^4 + \mu_2 \Delta^2 + \mu_3 = 0 \quad (59)$$

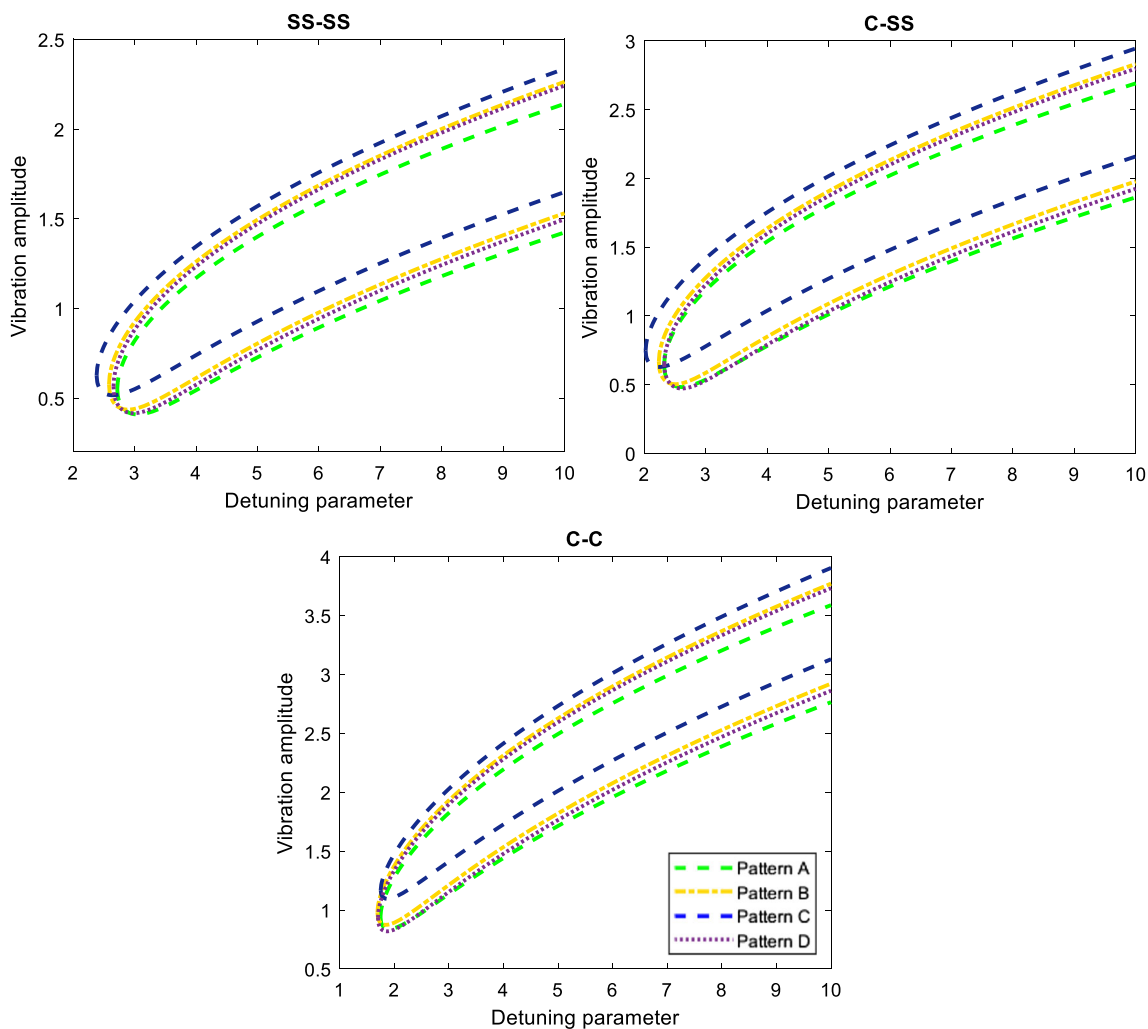


Fig. 8 Surface elastic frequency response of FG porous silicon nanobeams under subharmonic excitation corresponding to various porosity dispersion patterns ($h = 5 \text{ nm}$, $\Gamma_p = 0.6$, $\bar{F} = 0.4$)

where

$$\begin{aligned} \mu_1 &= \frac{81\tilde{\alpha}_1^2}{\tilde{\omega}_1^2}, \quad \mu_2 = \frac{243\tilde{\alpha}_1^2 a^2}{16\tilde{\omega}_1^2} - \frac{18\tilde{\alpha}_1 \Gamma}{\tilde{\omega}_1} \\ \mu_3 &= 9\vartheta^2 + \Gamma^2 + \frac{81\tilde{\alpha}_1^2 a^4}{64\tilde{\omega}_1^2} - \frac{9\tilde{\alpha}_1 a^2 \Gamma}{4\tilde{\omega}_1}. \end{aligned} \tag{60}$$

The solution of Eq. (59) is the size-dependent amplitude response for an FG porous silicon nanobeam subjected to subharmonic excitation.

4 Results and discussion

Herein, selected numerical results for the nonlinear secondary resonance of FG porous silicon nanobeams under harmonic excitation is analyzed in the presence of free

surface energy effects and corresponding to simply supported–simply supported (SS–SS), clamped–simply supported (C–SS) and clamped–clamped (C–C) boundary conditions. The mechanical properties and surface elastic constants of silicon material are given in Table 1. It is assumed that $L/h = 20$, $b = h$, and $\vartheta = 0.2$. In addition, this point should be noted that the present analysis is based on this assumption that the values of frequencies corresponding to different vibration modes are not within the range that leads to internal resonance.

To check the validity as well as accuracy of the current investigation, the natural frequency of silicon nanobeams with different thicknesses and boundary conditions in the presence of the surface stress are obtained and compared to those reported by Ansari et al. [75] using generalized differential quadrature methodology. A very good agreement

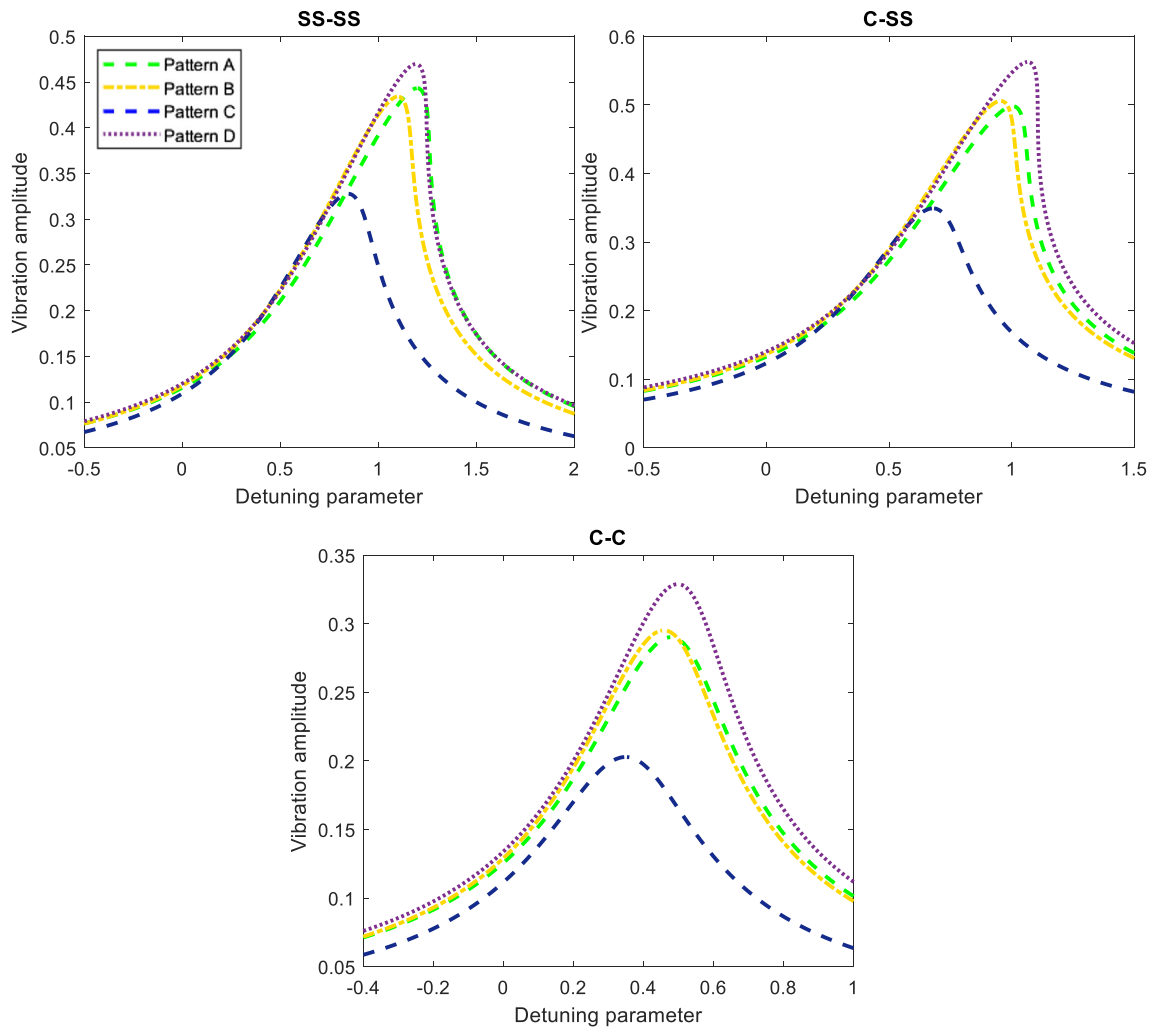


Fig. 9 Surface elastic frequency response of FG porous silicon nanobeams under superharmonic excitation corresponding to various porosity dispersion patterns ($h = 5 \text{ nm}$, $\Gamma_p = 0.6$, $\bar{F} = 0.4$)

is found which confirms the validity of the present solving process (Table 2).

In Figs. 4 and 5, the frequency response of porous silicon nanobeams with different thicknesses and uniform porosity dispersion (pattern A) is displayed corresponding to the subharmonic and superharmonic excitations, respectively. It is revealed that due to the higher surface to volume ratio for a nanobeam with lower thickness, reduction in the value of beam thickness causes to enhance the difference between the classical and non-classical frequency responses. In the case of superharmonic excitation, it is seen that the surface stress effect leads to decrease the both height of jump phenomenon and the associated non-linearity effect to the hardening direction. As a result, the excitation frequency associated with the both bifurcation points increases by taking the surface stress effect into account. These anticipations are more significant for the

SS–SS boundary conditions. Regarding the subharmonic excitation, it is seen that the surface stress effect leads to increase the value of the excitation frequency at the joint point of the two branches of the frequency response curve. However, by moving from SS–SS boundary conditions to C–C ones, the significance of this effect diminishes.

Figures 6 and 7 depict the amplitude-response of porous silicon nanobeams with different thicknesses and uniform porosity dispersion (pattern A) corresponding to the superharmonic and subharmonic excitations, respectively. It is found that for the subharmonic excitation, within a specific range of the excitation amplitude, the nanobeam is excited, and this range shifts to higher excitation amplitude with higher area by incorporating the surface free energy effects, especially for SS–SS boundary conditions. In addition, for the superharmonic excitation, by taking the surface stress effect into account, the excitation amplitude

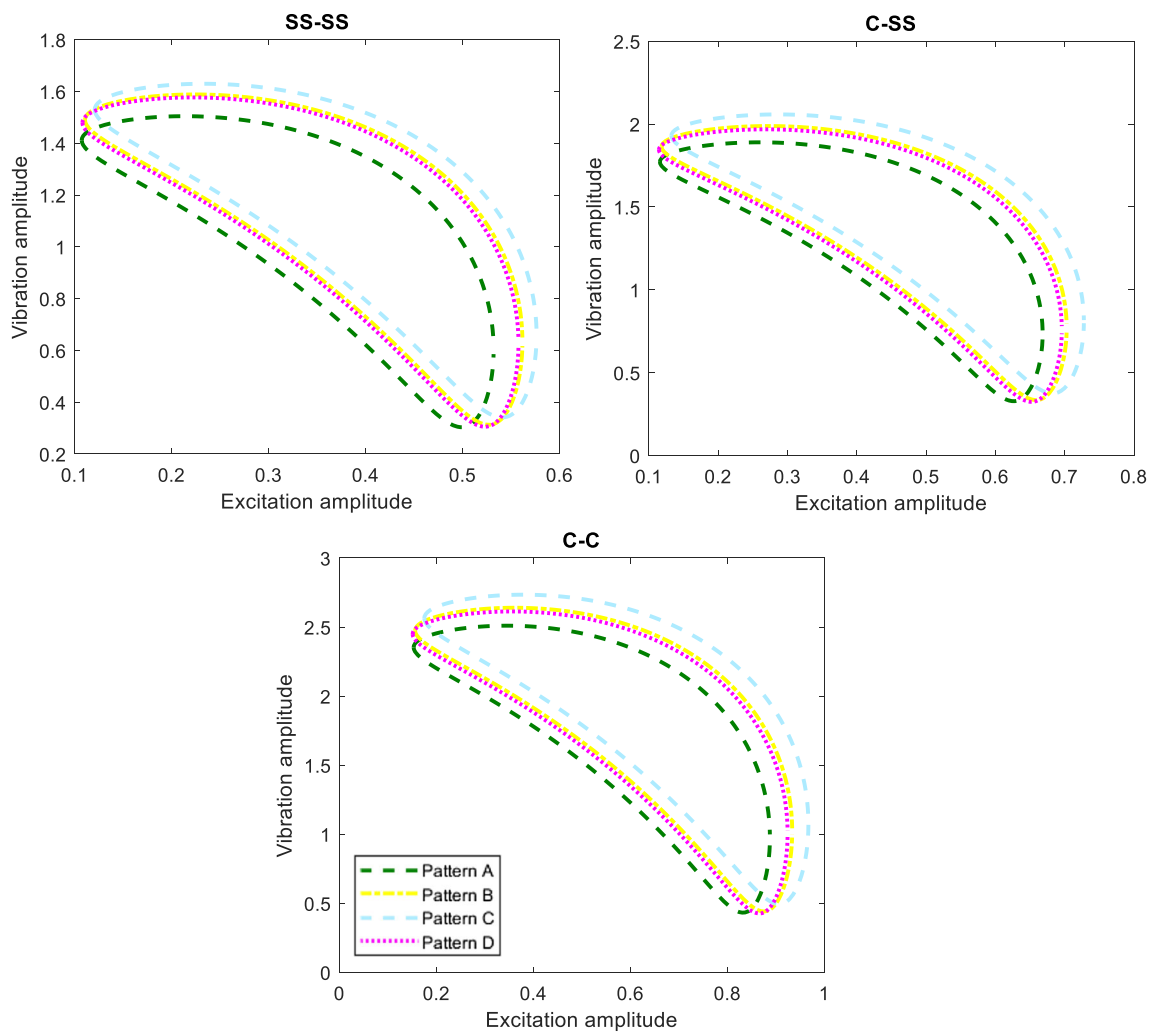


Fig. 10 Surface elastic amplitude response of FG porous silicon nanobeams under subharmonic excitation corresponding to various porosity dispersion patterns ($h = 5$ nm, $\Gamma_p = 0.6$, $\Gamma = 5$)

associated with the peak of vibration amplitude enhances. Also, the surface stress effect causes the bifurcation points occur at higher excitation amplitude.

The influence of the porosity dispersion pattern on the frequency response of FG porous silicon nanobeams with different end supports including surface stress effects is shown in Figs. 8 and 9 corresponding to the subharmonic and superharmonic excitations, respectively. In the subharmonic case, it is revealed that the value of the excitation frequency at the joint point of the two branches of the frequency-response curve for patterns D and C is maximum and minimum, respectively. However, this difference between various patterns of the porosity dispersion becomes negligible by changing the boundary conditions from SS–SS ones to C–C ones. In the superharmonic case, it is observed that the peak of the oscillation amplitude and the associated excitation frequency are maximum and

minimum, respectively, for pattern D and pattern C of the porosity dispersion. This prediction is the same for all types of end supports.

Figures 10 and 11 demonstrate the influence of the porosity dispersion pattern on the amplitude response of FG porous silicon nanobeams with different end supports including surface stress effects is corresponding to the subharmonic and superharmonic excitations, respectively. In the subharmonic case, it is found that by changing the porosity dispersion pattern from pattern A to pattern D, from pattern D to pattern B, and from pattern B to pattern C, the specific range of the excitation amplitude corresponding to which the FG porous nanobeams is excited, shifts to a higher value. In the superharmonic case, it is seen that the excitation amplitude associated with the peak of the oscillation amplitude is maximum and minimum for FG porous nanobeams with patterns C and A, respectively.

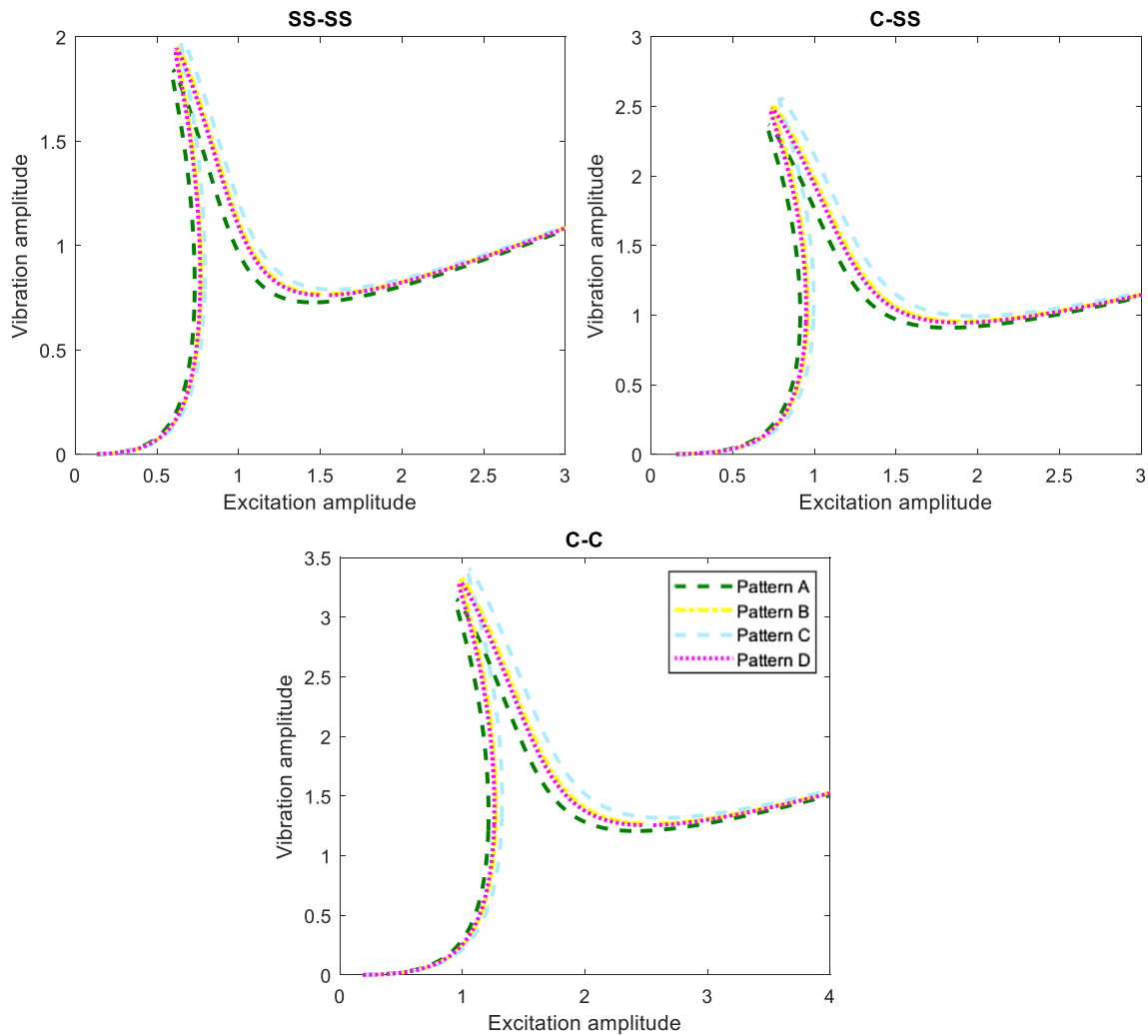


Fig. 11 Surface elastic amplitude-response of FG porous silicon nanobeams under superharmonic excitation corresponding to various porosity dispersion patterns ($h = 5 \text{ nm}$, $\Gamma_p = 0.6$, $\Gamma = 5$)

In Figs. 12 and 13, the influence of porosity coefficient on the frequency response of porous silicon nanobeams with uniform porosity dispersion (pattern A) and various end supports incorporating surface stress effects is shown corresponding to the subharmonic and superharmonic excitations, respectively. In the subharmonic case, it can be observed that by increasing the porosity coefficient, the value of the excitation frequency at the joint point of the two branches of the frequency-response curve reduces. This anticipation becomes more prominent by changing the boundary conditions from C–C ones to SS–SS ones. In the superharmonic case, it is indicated that an increment in the value of porosity coefficient leads to decrease the peak of the oscillation amplitude and the associated excitation frequency.

The influence of porosity coefficient on the amplitude response of porous silicon nanobeams with uniform

porosity dispersion (pattern A) and various end supports incorporating surface stress effects is illustrated in Figs. 14 and 15 corresponding to the subharmonic and superharmonic excitations, respectively. In the subharmonic case, it is revealed that by increasing the value of porosity coefficient, the specific range of the excitation amplitude corresponding to which the porous silicon nanobeam is excited, shifts to higher value. In the superharmonic case, the increase in the value of porosity coefficient results in an increment in the excitation amplitude associated with the peak of the oscillation amplitude. These observations are similar for all types of boundary conditions.

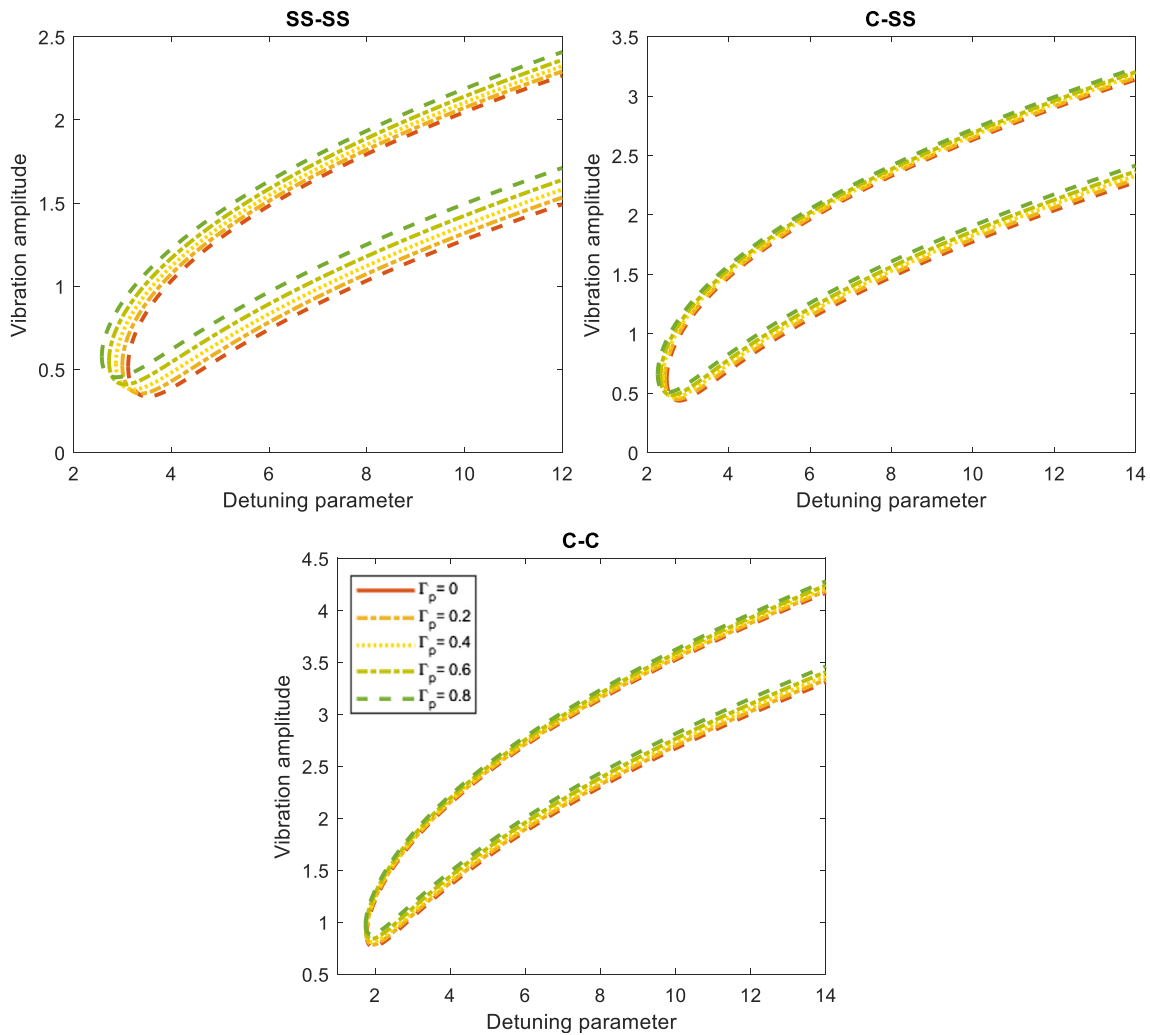


Fig. 12 Surface elastic frequency response of FG porous silicon nanobeams under subharmonic excitation corresponding to various porosity coefficients ($h = 5$ nm, pattern A, $\tilde{F} = 0.4$)

5 Concluding remarks

The prime aim of the current study was to investigate the nonlinear secondary resonance of hard excited FG porous silicon nanobeams in the presence of the surface free energy effects. Consequently, the Gurtin–Murdoch theory of elasticity was applied to the classical beam theory to construct a non-classical beam model having the capability to take surface stress effects into consideration. With the aid of the multiple time-scales method together with the Galerkin technique, the frequency response and amplitude response of the FG porous silicon nanobeams were obtained based upon the developed surface elastic beam model.

It was shown that due to the higher surface to volume ratio for a nanobeam with lower thickness, reduction in the value of beam thickness causes to enhance the difference between the classical and non-classical predictions for the nonlinear secondary resonance response. In the case of superharmonic excitation, it was revealed that the surface stress effect leads to decrease the both height of jump phenomenon and the associated nonlinearity effect to the hardening direction. As a result, the excitation frequency associated with the both bifurcation points increases by taking the surface stress effect into account. Regarding the subharmonic excitation, it was observed that the surface stress effect leads to increase the value of the excitation

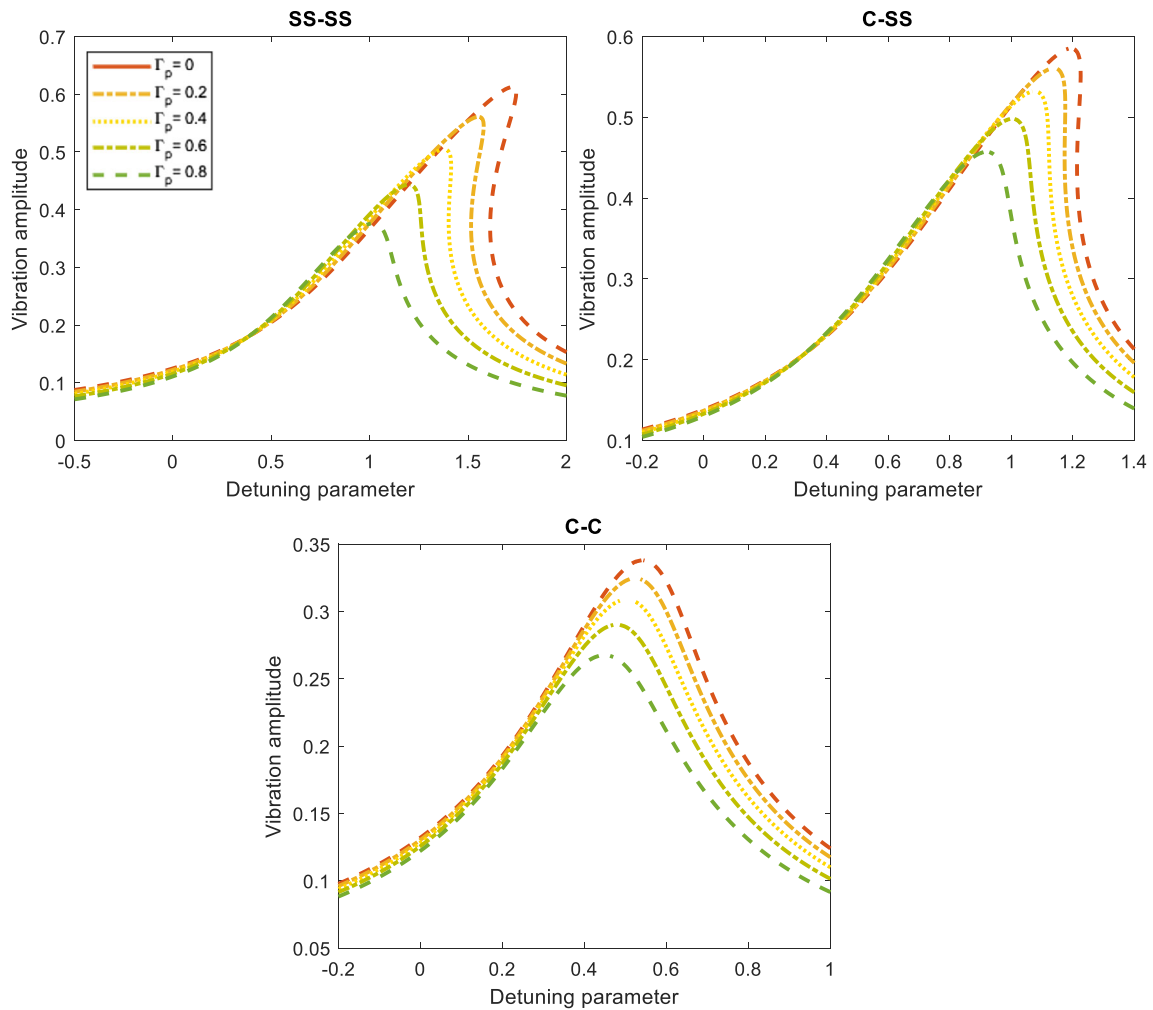


Fig. 13 Surface elastic frequency response of FG porous silicon nanobeams under superharmonic excitation corresponding to various porosity coefficients ($h = 5$ nm, pattern A, $\bar{F} = 0.4$)

frequency at the joint point of the two branches of the frequency-response curve.

In the subharmonic case, it was indicated that by changing the porosity dispersion pattern from pattern A to

pattern D, from pattern D to pattern B, and from pattern B to pattern C, the specific range of the excitation amplitude corresponding to which the FG porous nanobeams is excited, shifts to a higher value. In the superharmonic case,

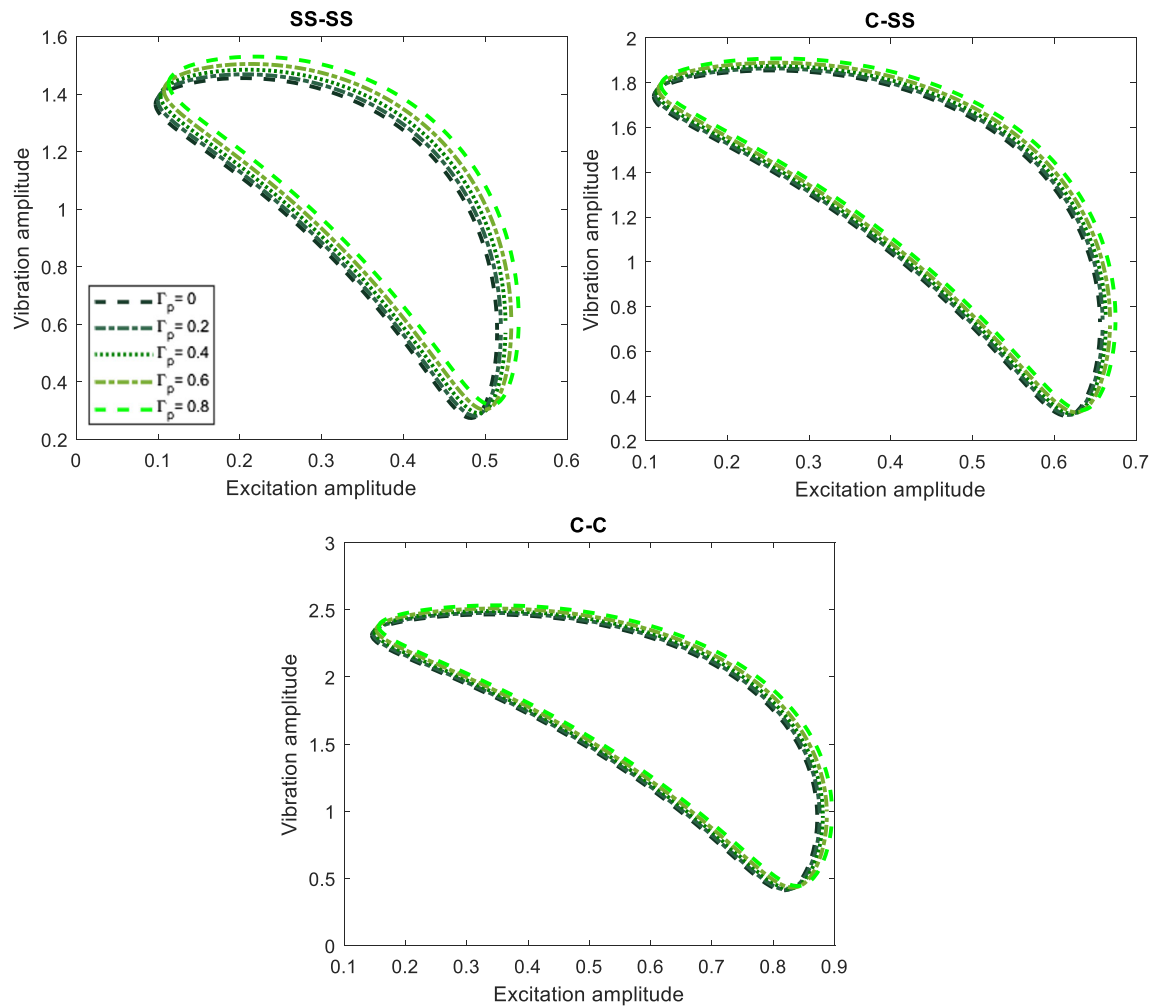


Fig. 14 Surface elastic amplitude response of FG porous silicon nanobeams under subharmonic excitation corresponding to various porosity coefficients ($h = 5$ nm, pattern A, $\Gamma = 5$)

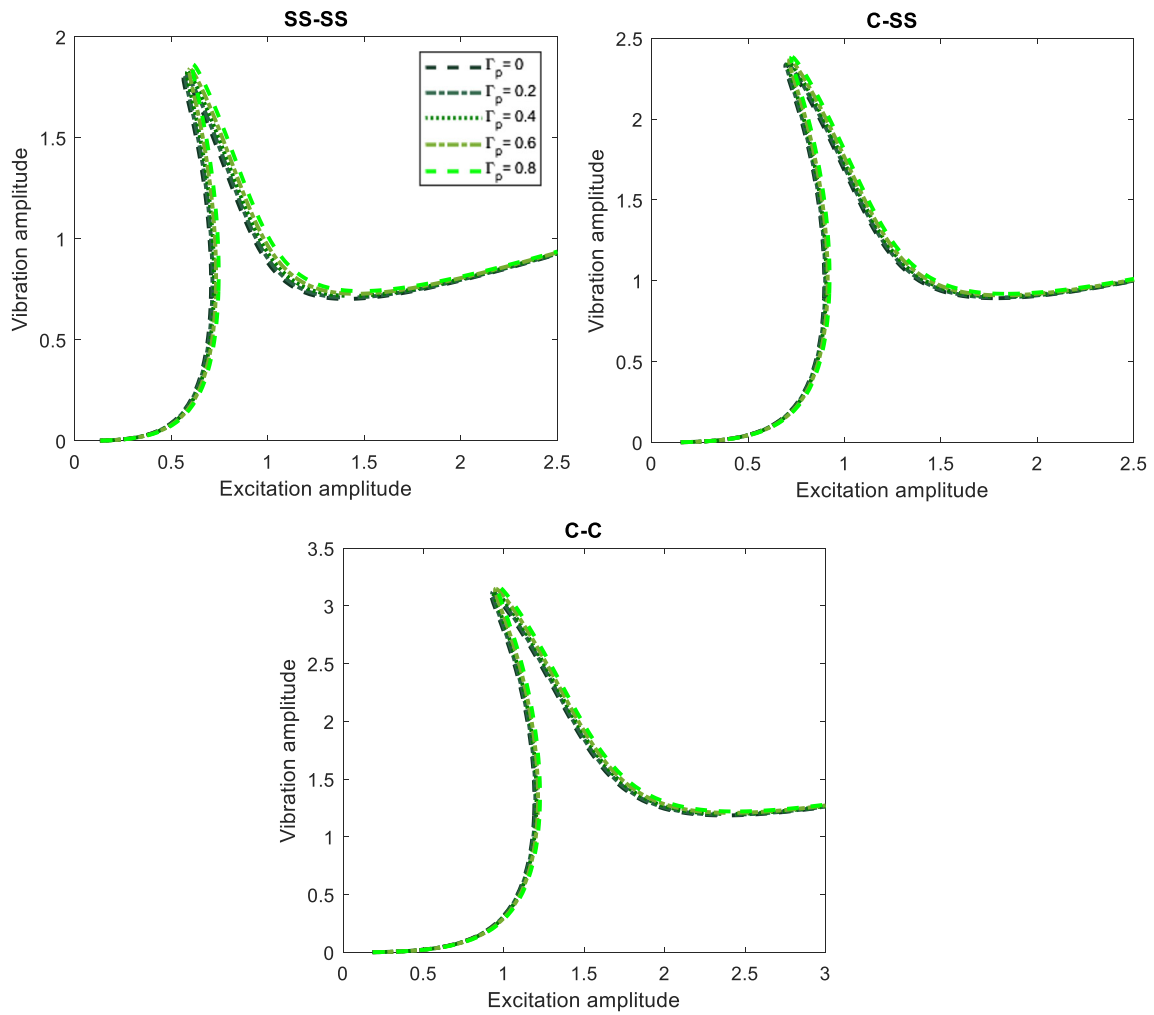


Fig. 15 Surface elastic amplitude-response of FG porous silicon nanobeams under superharmonic excitation corresponding to various porosity coefficients ($h = 5$ nm, pattern A, $\Gamma = 5$)

it was demonstrated that the excitation amplitude associated with the peak of the oscillation amplitude is maximum and minimum for FG porous nanobeams with porosity dispersion patterns C and A, respectively.

Acknowledgements This research work was financially supported by the science and technology research project in Jiangxi province department of education (NO: GJJ161120) and Key project of advantageous science and technology innovation team of Jiangxi province in 2017 (“5511” project) (NO: 20171BCB19001).

References

- Chen D, Kitipornchai S, Yang J (2016) Nonlinear free vibration of shear deformable sandwich beam with a functionally graded porous core. *Thin Walled Struct* 107:39–48
- Wang Y, Wu D (2017) Free vibration of functionally graded porous cylindrical shell using a sinusoidal shear deformation theory. *Aerosp Sci Technol* 66:83–91
- Wu D, Liu A, Huang Y, Huang Y, Pi Y, Gao W (2018) Dynamic analysis of functionally graded porous structures through finite element analysis. *Eng Struct* 165:287–301
- Karami B, Janghorban M, Li L (2018) On guided wave propagation in fully clamped porous functionally graded nanoplates. *Acta Astronaut* 143:380–390
- Sahmani S, Aghdam MM, Rabczuk T (2018) Nonlinear bending of functionally graded porous micro/nano-beams reinforced with graphene platelets based upon nonlocal strain gradient theory. *Compos Struct* 186:68–78
- Sahmani S, Aghdam MM, Rabczuk T (2018) A unified nonlocal strain gradient plate model for nonlinear axial instability of functionally graded porous micro/nano-plates reinforced with graphene platelets. *Mater Res Express* 5:045048
- Sahmani S, Aghdam MM, Rabczuk T (2018) Nonlocal strain gradient plate model for nonlinear large-amplitude vibrations of functionally graded porous micro/nano-plates reinforced with GPLs. *Compos Struct* 198:51–62
- Gao K, Gao W, Wu B, Wu D, Song C (2018) Nonlinear primary resonance of functionally graded porous cylindrical shells using the method of multiple scales. *Thin Walled Struct* 125:281–293
- Safaei B, Moradi-Dastjerdi R, Qin Z, Behdinan K, Chu F (2019) Determination of thermoelastic stress wave propagation in nanocomposite sandwich plates reinforced by clusters of carbon nanotubes. *J Sandw Struct Mater*. <https://doi.org/10.1177/1099636219848282>
- Safaei B, Moradi-Dastjerdi R, Behdinan K, Chu F (2019) Critical buckling temperature and force in porous sandwich plates with CNT-reinforced nanocomposite layers. *Aerosp Sci Technol* 91:175–185
- Safaei B, Moradi-Dastjerdi R, Behdinan K, Qin Z, Chu F (2019) Thermoelastic behavior of sandwich plates with porous polymeric core and CNT clusters/polymer nanocomposite layers. *Compos Struct* 226:111209
- Qin Z, Safaei B, Pang X, Chu F (2019) Traveling wave analysis of rotating functionally graded graphene platelet reinforced nanocomposite cylindrical shells with general boundary conditions. *Results Phys* 15:102752
- Qin Z, Zhao S, Pang X, Safaei B, Chu F (2020) A unified solution for vibration analysis of laminated functionally graded shallow shells reinforced by graphene with general boundary conditions. *Int J Mech Sci* 170:105341
- Sahmani S, Ansari R (2011) Nonlocal beam models for buckling of nanobeams using state-space method regarding different boundary conditions. *J Mech Sci Technol* 25:2365
- Wang Y-G, Lin W-H, Liu N (2013) Large amplitude free vibration of size-dependent circular microplates based on the modified couple stress theory. *Int J Mech Sci* 71:51–57
- Reddy JN, El-Borgi S, Romanoff J (2014) Non-linear analysis of functionally graded microbeams using Eringen’s non-local differential model. *Int J Non-Linear Mech* 67:308–318
- Sahmani S, Bahrami M, Ansari R (2014) Nonlinear free vibration analysis of functionally graded third-order shear deformable microbeams based on the modified strain gradient elasticity theory. *Compos Struct* 110:219–230
- Shojaeian M, Tadi Beni Y (2015) Size-dependent electromechanical buckling of functionally graded electrostatic nano-bridges. *Sens Actuators A Phys* 232:49–62
- Sahmani S, Aghdam MM, Bahrami M (2015) On the free vibration characteristics of postbuckled third-order shear deformable FGM nanobeams including surface effects. *Compos Struct* 121:377–385
- Ghorbani Shenaa A, Malekzadeh P, Mohebbpour S (2016) Free vibration of functionally graded quadrilateral microplates in thermal environment. *Thin Walled Struct* 108:122–137
- Togun N, Bagdatli SM (2016) Size dependent vibration of the tensioned nanobeam based on the modified couple stress theory. *Compos Part B: Eng* 97:255–261
- Sahmani S, Aghdam MM, Bahrami M (2017) An efficient size-dependent shear deformable shell model and molecular dynamics simulation for axial instability analysis of silicon nanoshells. *J Mol Graph Model* 77:263–279
- Wang CM, Zhang H, Challamel N, Duan WH (2017) On boundary conditions for buckling and vibration of nonlocal beams. *Eur J Mech A/Solids* 61:73–81
- Sahmani S, Aghdam MM (2017) Size dependency in axial postbuckling behavior of hybrid FGM exponential shear deformable nanoshells based on the nonlocal elasticity theory. *Compos Struct* 166:104–113
- Sahmani S, Aghdam MM (2017) Nonlinear instability of hydrostatic pressurized hybrid FGM exponential shear deformable nanoshells based on nonlocal continuum elasticity. *Compos Part B Eng* 114:404–417
- Sahmani S, Aghdam MM (2017) Temperature-dependent non-local instability of hybrid FGM exponential shear deformable nanoshells including imperfection sensitivity. *Int J Mech Sci* 122:129–142
- Guo J, Chen J, Pan E (2017) Free vibration of three-dimensional anisotropic layered composite nanoplates based on modified couple-stress theory. *Physica E* 87:98–106
- Sahmani S, Aghdam MM (2017) Size-dependent nonlinear bending of micro/nano-beams made of nanoporous biomaterials including a refined truncated cube cell. *Phys Lett A* 381:3818–3830
- Sahmani S, Aghdam MM (2017) Nonlinear vibrations of pre- and post-buckled lipid supramolecular micro/nano-tubules via non-local strain gradient elasticity theory. *J Biomech* 65:49–60
- Sahmani S, Aghdam MM (2018) Nonlocal strain gradient beam model for postbuckling and associated vibrational response of lipid supramolecular protein micro/nano-tubules. *Math Biosci* 295:24–35
- Attia MA, Abdel Rahman AA (2018) On vibrations of functionally graded viscoelastic nanobeams with surface effects. *Int J Eng Sci* 127:1–32
- Akgoz B, Civalek O (2018) Vibration characteristics of embedded microbeams lying on a two-parameter elastic foundation in thermal environment. *Compos Part B Eng* 150:68–77

33. Shahsavari D, Karami B, Li L (2018) Damped vibration of a graphene sheet using a higher-order nonlocal strain-gradient Kirchhoff plate model. *C R Mec* 346:1216–1232
34. Sahmani S, Aghdam MM (2018) Boundary layer modeling of nonlinear axial buckling behavior of functionally graded cylindrical nanoshells based on the surface elasticity theory. *Iran J Sci Technol Trans Mech Eng* 42:229–245
35. Imani Aria A, Biglari H (2018) Computational vibration and buckling analysis of microtubule bundles based on nonlocal strain gradient theory. *Appl Math Comput* 321:313–332
36. Sahmani S, Fattahi AM, Ahmed NA (2019) Size-dependent nonlinear forced oscillation of self-assembled nanotubules based on the nonlocal strain gradient beam model. *J Braz Soc Mech Sci Eng* 41:239
37. Zhang H, Challamel N, Wang CM, Zhang YP (2019) Exact and nonlocal solutions for vibration of multiply connected bar-chain system with direct and indirect neighbouring interactions. *J Sound Vib* 443:63–73
38. Sahmani S, Aghdam MM (2019) Nonlocal electrothermomechanical instability of temperature-dependent FGM nanopanels with piezoelectric facesheets. *Iran J Sci Technol Trans Mech Eng* 43:579–593
39. Trabelssi M, El-Borgi S, Fernandes R, Ke L-L (2019) Nonlocal free and forced vibration of a graded Timoshenko nanobeam resting on a nonlinear elastic foundation. *Compos Part B Eng* 157:331–349
40. Sahmani S, Safaei B (2019) Nonlinear free vibrations of bi-directional functionally graded micro/nano-beams including nonlocal stress and microstructural strain gradient size effects. *Thin Walled Struct* 140:342–356
41. Sahmani S, Safaei B (2019) Nonlocal strain gradient nonlinear resonance of bi-directional functionally graded composite micro/nano-beams under periodic soft excitation. *Thin Walled Struct* 143:106226
42. Glabisz W, Jarczewska K, Holubowski R (2019) Stability of Timoshenko beams with frequency and initial stress dependent nonlocal parameters. *Arch Civ Mech Eng* 19:1116–1126
43. Sahmani S, Fattahi AM, Ahmed NA (2019) Analytical mathematical solution for vibrational response of postbuckled laminated FG-GPLRC nonlocal strain gradient micro-/nanobeams. *Eng Comput* 35:1173–1189
44. Martin O (2019) Nonlocal effects on the dynamic analysis of a viscoelastic nanobeam using a fractional Zener model. *Appl Math Model* 73:637–650
45. Qian D, Shi Z, Ning C, Wang J (2019) Nonlinear bandgap properties in a nonlocal piezoelectric phononic crystal nanobeam. *Phys Lett A* 383:3101–3107
46. Sahmani S, Madyira DM (2019) Nonlocal strain gradient nonlinear primary resonance of micro/nano-beams made of GPL reinforced FG porous nanocomposite materials. *Mech Based Des Struct Mach*. <https://doi.org/10.1080/15397734.2019.1695627>
47. Safaei B, Khoda FH, Fattahi AM (2019) Non-classical plate model for single-layered graphene sheet for axial buckling. *Advances in Nano Research* 7:265–275
48. Sahmani S, Fattahi AM, Ahmed NA (2019) Analytical treatment on the nonlocal strain gradient vibrational response of postbuckled functionally graded porous micro-/nanoplates reinforced with GPL. *Eng Comput*. <https://doi.org/10.1007/s00366-019-00782-5>
49. Gurtin ME, Murdoch AI (1975) A continuum theory of elastic material surface. *Arch Ration Mech Anal* 57:291–323
50. Gurtin ME, Murdoch AI (1978) Surface stress in solids. *Int J Solids Struct* 14:431–440
51. Wang G-F, Feng X-Q (2007) Effects of surface elasticity and residual surface tension on the natural frequency of microbeams. *Appl Phys Lett* 90:231904
52. Lü CF, Chen WQ, Lim CW (2009) Elastic mechanical behavior of nano-scaled FGM films incorporating surface energies. *Compos Sci Technol* 69:1124–1130
53. Fu Y, Zhang J, Jiang Y (2010) Influences of surface energies on the nonlinear static and dynamic behaviors of nanobeams. *Physica E* 42:2268–2273
54. Sahmani S, Ansari R (2011) Surface stress effects on the free vibration behavior of nanoplates. *Int J Eng Sci* 49:1204–1215
55. Sahmani S, Ansari R (2011) Bending behavior and buckling of nanobeams including surface stress effects corresponding to different beam theories. *Int J Eng Sci* 49:1244–1255
56. Gao F, Cheng Q, Luo J (2014) Mechanics of nanowire buckling on elastomeric substrates with consideration of surface stress effects. *Physica E* 64:72–77
57. Sahmani S, Bahrami M, Ansari R (2014) Surface energy effects on the free vibration characteristics of postbuckled third-order shear deformable nanobeams. *Compos Struct* 116:552–561
58. Asemi SR, Farajpour A (2014) Decoupling the nonlocal elasticity equations for thermo-mechanical vibration of circular graphene sheets including surface effects. *Physica E* 60:80–90
59. Sahmani S, Bahrami M, Aghdam MM, Ansari R (2014) Surface effects on the nonlinear forced vibration response of third-order shear deformable nanobeams. *Compos Struct* 118:149–158
60. Ghorbanpour Arani A, Abdollahian M, Jalaei MH (2015) Vibration of bioliquid-filled microtubules embedded in cytoplasm including surface effects using modified couple stress theory. *J Theor Biol* 367:29–38
61. Sahmani S, Aghdam MM, Bahrami M (2015) Nonlinear buckling and postbuckling behavior of cylindrical nanoshells subjected to combined axial and radial compressions incorporating surface stress effects. *Compos Part B Eng* 79:676–691
62. Sahmani S, Aghdam MM, Akbarzadeh AH (2016) Size-dependent buckling and postbuckling behavior of piezoelectric cylindrical nanoshells subjected to compression and electrical load. *Mater Des* 105:341–351
63. Sahmani S, Aghdam MM, Bahrami M (2017) Surface free energy effects on the postbuckling behavior of cylindrical shear deformable nanoshells under combined axial and radial compressions. *Meccanica* 52:1329–1352
64. Lu L, Guo X, Zhao J (2018) On the mechanics of Kirchhoff and Mindlin plates incorporating surface energy. *Int J Eng Sci* 124:24–40
65. Sun J, Wang Z, Zhou Z, Xu X, Lim CW (2018) Surface effects on the buckling behaviors of piezoelectric cylindrical nanoshells using nonlocal continuum model. *Appl Math Model* 59:341–356
66. Sarafraz A, Sahmani S, Aghdam MM (2019) Nonlinear secondary resonance of nanobeams under subharmonic and superharmonic excitations including surface free energy effects. *Appl Math Model* 66:195–226
67. Dong S, Zhu C, Chen Y, Zhao J (2019) Buckling behaviors of metal nanowires encapsulating carbon nanotubes by considering surface/interface effects from a refined beam model. *Carbon* 141:348–362
68. Sahmani S, Fattahi AM, Ahmed NA (2019) Radial postbuckling of nanoscaled shells embedded in elastic foundations based on Ru's surface stress elasticity theory. *Mech Based Des Struct Mach* 47:787–806
69. Lu L, Guo X, Zhao J (2019) A unified size-dependent plate model based on nonlocal strain gradient theory including surface effects. *Appl Math Model* 68:583–602
70. Yang Y, Hu Z-L, Li X-F (2020) Nanoscale mode-III interface crack in a bimaterial with surface elasticity. *Mech Mater* 140:103246
71. Sahmani S, Fattahi AM, Ahmed NA (2020) Surface elastic shell model for nonlinear primary resonant dynamics of FG porous

- nanoshells incorporating modal interactions. *Int J Mech Sci* 165:105203
72. Roberts AP, Garboczi EJ (2001) Elastic moduli of model random three-dimensional closed-cell cellular solids. *Acta Mater* 49:189–197
73. Miller RE, Shenoy VB (2000) Size-dependent elastic properties of nanosized structural elements. *Nanotechnology* 11:139–147
74. Zhu R, Pan E, Chung PW, Cai X, Liew KM, Buldum A (2006) Atomistic calculation of elastic moduli in strained silicon. *Semicond Sci Technol* 21:906–911
75. Ansari R, Mohammadi V, Shojaei MF, Gholami R, Sahmani S (2014) On the forced vibration analysis of Timoshenko nano-beams based on the surface stress elasticity theory. *Compos Part B Eng* 60:158–166

Publisher's Note Springer Nature remains neutral with regard to jurisdictional claims in published maps and institutional affiliations.